Ozone production efficiency and NO_x depletion in an urban plume: Interpretation of field observations and implications for evaluating O_3-NO_x-VOC sensitivity

Rahul A. Zaveri,[1] Carl M. Berkowitz,[1] Lawrence I. Kleinman,[2] Stephen R. Springston,[2] Paul V. Doskey,[3] William A. Lonneman,[4] and Chester W. Spicer[5]

Received 5 November 2002; revised 28 March 2003; accepted 20 May 2003; published 31 July 2003.

[1] Ozone production efficiency (OPE) can be defined as the number of ozone (O_3) molecules photochemically produced by a molecule of NO_x ($NO + NO_2$) before it is lost from the $NO_x - O_3$ cycle. Here we consider observational and modeling techniques to evaluate various operational definitions of OPEs using aircraft and surface measurements taken as part of the 1999 Southern Oxidant Study field campaign in Nashville, Tennessee. A key tool in our analysis is a Lagrangian box model, which is used to quantitatively describe the effects of emissions, dilution, dry deposition, and photochemistry in an urban air parcel as it was advected downwind. After evaluating the model using the observed downwind concentrations of several key species, we show that the modeled NO_x oxidation and O_3 production rates as well as the associated instantaneous and cumulative OPEs depend on the time of day and the photochemical age of the air parcel. The observation-based OPEs are found to be consistent with the modeled values with the expected biases. A model sensitivity study suggests that downwind O_3 concentrations in the Nashville plume are more sensitive to NO_x emissions than anthropogenic VOC emissions. Because the OPE exhibits a nonlinear dependence on emissions and meteorological effects, it would be difficult to rely only on observations to map out the nonlinear response of O_3 to a wide span of NO_x and VOC emission changes. Properly constrained and well-evaluated models using a variety of observations are therefore necessary to reliably predict O_3-NO_x-VOC sensitivity for designing effective O_3 control strategies. *INDEX TERMS:* 0317 Atmospheric Composition and Structure: Chemical kinetic and photochemical properties; 0345 Atmospheric Composition and Structure: Pollution—urban and regional (0305); 0368 Atmospheric Composition and Structure: Troposphere—constituent transport and chemistry; 3329 Meteorology and Atmospheric Dynamics: Mesoscale meteorology; 3367 Meteorology and Atmospheric Dynamics: Theoretical modeling; *KEYWORDS:* air pollution, Lagrangian modeling, aircraft measurements

Citation: Zaveri, R. A., C. M. Berkowitz, L. I. Kleinman, S. R. Springston, P. V. Doskey, W. A. Lonneman, and C. W. Spicer, Ozone production efficiency and NO_x depletion in an urban plume: Interpretation of field observations and implications for evaluating O_3-NO_x-VOC sensitivity, *J. Geophys. Res.*, *108*(D14), 4436, doi:10.1029/2002JD003144, 2003.

1. Introduction

[2] Urban and rural surface ozone has been the subject of a number of major air quality field campaigns in North America and Europe [*Solomon et al.*, 2000]. A practical goal behind these studies has been to elucidate the relationship between volatile organic compounds (VOCs), nitrogen oxides ($NO_x = NO + NO_2$), sum of all odd-nitrogen species (NO_y) and O_3 [*Altshuller*, 1986; *Trainer et al.*, 2000, and references therein]. In the presence of solar radiation and VOCs, a molecule of NO_x could catalytically produce either zero, one, or several molecules of O_3 before it is removed from the system by oxidation reactions forming nitric acid (HNO_3), nitrous acid (HONO), peroxy acyl nitrates (PANs), and other organic nitrates, which are collectively denoted as 'NO_z,' and often calculated as ($NO_y - NO_x$). Due to rapid photolysis of HONO back to NO in the presence of solar radiation, it is a temporary reservoir of NO_x during the daytime, and PAN is also likely to thermally decompose to produce NO_2. While these species are lumped as NO_z, they do not necessarily remove NO_x permanently. Furthermore, in a boundary layer air parcel, the species are simultaneously subjected to dilution, dry deposition, and fresh

[1]Atmospheric Sciences and Global Change Division, Pacific Northwest National Laboratory, Richland, Washington, USA.
[2]Environmental Sciences Department, Brookhaven National Laboratory, Upton, New York, USA.
[3]Environmental Research Division, Argonne National Laboratory, Argonne, Illinois, USA.
[4]National Exposure Research Laboratory, Senior Environmental Employment Program, U.S. Environmental Protection Agency, Research Triangle Park, North Carolina, USA.
[5]Atmospheric Science and Applied Technology Department, Battelle Memorial Institute, Columbus, Ohio, USA.

Copyright 2003 by the American Geophysical Union.
0148-0227/03/2002JD003144$09.00

emissions as they are advected away from an urban source region. Here the term air parcel is understood from a Lagrangian viewpoint as a geometric volume of air that is approximately homogeneous in the pollutant mixing ratios, and which has been traveling through the boundary layer with approximately uniform wind speed and direction. However, with time an air parcel invariably experiences dilution due to wind shear and turbulence, and eventually loses its "original identity" as it blends with adjacent air parcels. The number of ozone molecules produced by a molecule of NO_x in an air parcel before it is lost from the NO_x-O_3 cycle due to oxidation and dry deposition is called the ozone production efficiency (OPE). This term was first defined by *Liu et al.* [1987] who used a photochemical box model to calculate the OPE at Niwot Ridge, a rural mountain site in Colorado. They showed that the OPE changed nonlinearly with change in NO_x, with O_3 produced more efficiently at low concentrations of NO_x and vice versa, and found evidence of this inverse, nonlinear behavior in the net daily O_3 changes observed at Niwot Ridge as a function of NO_x concentrations.

[3] OPEs have been subsequently estimated in rural areas and urban and power plant plumes from field measurements as the slope of correlation of O_3 with NO_z [*Trainer et al.*, 1993, 1995; *Kleinman et al.*, 1994; *Olszyna et al.*, 1994; *Imhoff et al.*, 1995; *Nunnermacker et al.*, 2000; *Rickard et al.*, 2002], and as the ratio of flux or cross-plume integrals of "excess" O_3 to "excess" NO_z (or NO_x consumed) in a plume transect, where excess is defined relative to the crosswind background conditions [*Gillani et al.*, 1998a; *Nunnermacker et al.*, 1998; *Ryerson et al.*, 1998]. These studies report OPEs between 2 and 12, with low values typically observed in plumes containing high-NO_x concentrations and vice versa. Although most of the NO_x lost from the catalytic cycle is converted into NO_z, neglecting the subsequent depositional loss of NO_z species in the measurement-based approaches results in overestimation of the OPE [*Trainer et al.*, 2000; *Rickard et al.*, 2002]. Other factors such as dilution, cloud-venting, and fresh emissions also complicate the interpretation of measured OPEs. To this end, the measured OPEs have been "corrected" for mixing and dry deposition effects by ratioing the measurements to coemitted "tracers" such as SO_2 and CO, or approximating them as first-order processes and estimating their e-folding times from meteorological and chemical measurements [*Gillani et al.*, 1998b; *Nunnermacker et al.*, 1998; *Ryerson et al.*, 1998; *St. John et al.*, 1998]. Conversely, *Sillman et al.* [1998] compared correlations between O_3, NO_z, and peroxides calculated from observations in the vicinity of Nashville, Tennessee, with those obtained from a three-dimensional (3-D) photochemical Eulerian model to understand the effects of the removal processes of NO_z on the OPE. More recently, *Sillman* [2000] employed a 2-D Lagrangian model to further investigate OPE and the rate of photochemical removal of NO_x using the power plant plume measurements collected by *Ryerson et al.* [1998] in the Nashville area. Although there was considerable discrepancy between the initial model results and measurements, a modified model scenario, constructed by adjusting emission and mixing rates, performed satisfactorily and helped gain a deeper insight into the nonlinear chemical and dynamical processes affecting the OPE and loss of NO_x. In another recent study, *Kleinman et al.* [2002] employed a constrained steady state box model in a Lagrangian fashion to estimate evolution of the instantaneous OPEs as a function of time in the Phoenix metropolitan area.

[4] The present study reports on the analysis and interpretation of the observations made in the Nashville urban plume during the 1999 Southern Oxidant Study (SOS). SOS is a long-term program focusing on the management of photochemical oxidants in the southern U.S. The 1999 Nashville campaign focused on obtaining an improved understanding of the processes that control the formation and distribution of fine particles and ozone. This large campaign included four aircrafts and an extensive set of ground-based chemical and meteorological observations made at Dickson, Tennessee (53 km WNW of Nashville, an upwind, rural site), at the James K. Polk Building in downtown Nashville (110 m above the street, providing a record of the urban emission mix) and at the Cornelia Fort Air Park, 8 km NE of Nashville, a downwind, urban site.

1.1. Scope

[5] Our analysis is focused on the airborne measurements made in the plume by Battelle's Grumman Gulfstream-1 aircraft (G-1) on the afternoon of 22 June 1999. The plume centerline and air parcel "age" as a function of downwind distance from the source area are derived from back-trajectories calculated using wind profiler measurements taken at the Cornelia Fort site. Measurements along the plume are used to estimate various observation-based OPEs. A Lagrangian box model, that accounts for chemistry, dilution, dry deposition, and emissions, is used to explain the observations in a selected urban air parcel that had passed over the downtown area in the morning, and was later sampled by the G-1 in the afternoon. The initial and boundary conditions and other model inputs are carefully selected from a combination of aircraft data and ground measurements. After satisfactorily evaluating the model, it is used to estimate the "instantaneous" and "cumulative" OPEs, and the associated O_3 production and NO_x loss rates in the selected air parcel as it was advected downwind. We conclude the analysis with a sensitivity study to investigate the effects of dilution and changes in NO_x and VOC emissions on the downwind O_3 concentration and its production efficiency. At the end, we discuss the implications of the findings of this study for evaluating the O_3-NO_x-VOC sensitivity for designing effective O_3 control strategies in urban areas.

2. Experiment

[6] According to the 2000 U.S. Census Bureau, the population of the eight-county Nashville Metropolitan Statistical Area is about 1.23 million, with nearly 569,000 people living in the Nashville city. Downtown Nashville is surrounded by a commercial area within a radius of about 6 km, which experiences heavy traffic that peaks during the morning and afternoon rush hours. In this study, we use the G-1 aircraft measurements in the Nashville urban plume in conjunction with measurements made at the Polk Building and Cornelia Fort Air Park ground sites to characterize the

photochemical production of O_3 from the emissions of NO_x and VOCs.

2.1. Ground-Based Measurements

[7] The Polk Building is located in the center of the downtown where chemical sampling was performed from a 5-m tower attached to the roof of the building, 106 m above street level. This site was managed by Tennessee Valley Authority personnel, and measured O_3, NO_x, NO_y, and CO concentrations as well as standard meteorological variables. The values for NO_y represent all NO_x and higher-oxidized nitrogen species in both the gas and aerosol phases. Further information about instrumentation at the Polk Building site is given by *Olszyna* [2002]. Air samples for the analysis of nonmethane organic compounds (NMOCs) were also collected in 6-L Summa® passivated stainless steel canisters (Scientific Instrumentation Specialists, Moscow, ID) on the roof of the Polk Building using an automated sampler described in detail by *Doskey and Bialk* [2001]. The sampler consisted of a Viton® diaphragm pump (KNF Neuberger, Inc., Trenton, NJ); a metal bellows metering valve (Nupro, Willoughby, OH), a 2-position, 3-port valve; a 10-port multiposition valve (VICI, Houston, TX); and a digital valve sequence programmer (VICI, Houston, TX). A 5-min sample was collected every 2 hours between 0700 and 1900 LT and every 3 hours between 1900 and 0700 LT. A comparison of the technique used in Nashville with a method in which a sample was passively collected in a canister yielded a sampling precision of 5–25% for a mixture of 25 C_2–C_8 hydrocarbons[*Doskey and Bialk*, 2001].

[8] The Cornelia Fort Air Park (CFA) is located 8–9 km to the northeast of the Polk Building site. With the prevailing wind direction (SW), CFA location serves as a downwind site. The area is mostly open and flat with some small stands of forest interspersed. This was the SOS 99 "super" chemistry site, which hosted several instruments from many institutions, and provided measurements of trace gases, aerosols, and vertical wind, relative humidity, and temperature profiles. The wind profiler measurements made at CFA are discussed by *Angevine et al.* [2003].

2.2. G-1 Measurement Instrumentation

[9] This section describes the measurement instrumentation onboard the G-1 aircraft. Oxides of nitrogen (NO, NO_2, and NO_y) were measured using a three-channel NO/O_3 chemiluminescence instrument, as previously described by *Daum et al.* [1996]. Again, the values for NO_y represent all NO_x and higher-oxidized nitrogen species in both the gas and aerosol phases. Detection limits for a 10-s averaging period were ~10, ~25, and ~100 pptv for nitric oxide (NO), nitrogen dioxide (NO_2), and total odd nitrogen (NO_y), respectively. All these nitrogen species were measured with a time resolution of <4 s. The zero-air artifact on the NO_y observations ranged between 0.36 and 0.74 ppbv; this is the signal above prereactor zero when sampling dry zero air, and is the worst case for background artifact from the converter. The heated glass inlet of the NO_y converter sampled from a 0.5-m length of 0.5-inch PFA tubing in an open split configuration. Some loss of HNO_3 and aerosol nitrate is possible in this configuration. Sensitivity of each channel was related to an NO standard in weekly ground calibrations and regular in-flight standard additions. The same standard was used to assess conversion efficiency for NO_2 (ground and in-flight) in the NO_2 and NO_y channels. Variability of NO sensitivity was 10–15% RSD over the course of this experiment. A lower uncertainty in the photolytic conversion of NO_2 suggests an aggregate uncertainty of <21% RSD for this species. Ozone was measured using a commercial UV absorption detector (Thermo Environmental Instruments, Model 49–100) with a detection limit of 5 ppb and a time resolution of ~10 s. Field and flight calibrations were done with the instrument's internal ozone source which was referenced in the laboratory to our NO standard using gas-phase titration. An estimated accuracy is 5% or 5 ppbv, whichever is greater. Periodic in-flight zeros were made using a charcoal trap. PAN was measured with an automated onboard gas chromatograph (Shimadzu Mini2 GC) using ^{63}Ni electron capture detection. The configuration was similar to that described by *Berkowitz et al.* [1998], except that a 1-mL gas sampling loop was employed and a sample was analyzed every 7.5 min. The estimated detection limit for PAN is 50 ppt with a precision better than 10%.

[10] Air samples for the analysis of NMOCs were collected aboard the G-1 aircraft in preevacuated 1.8-L Summa® passivated stainless steel canisters (Scientific Instrumentation Specialists, Moscow, ID). Air was drawn through a forward facing inlet outside the aircraft and pressurized in canisters using a metal bellows pump with a Viton® valve assembly (MB-151; Senior Flexonics, Inc., Sharon, MA). The canisters were attached to a stainless steel manifold and were pressurized to 25 psig over a period of 10–20 s. The sampling system was cleaned with humidified, ultra zero air in the laboratory at Argonne National Laboratory and was evaluated for sampling artifacts by simultaneously collecting several samples of ambient air at ground level with the aircraft sampling system and by passively collecting air in other canisters. Differences between the concentrations of C_2–C_8 hydrocarbons in samples collected by the two methods were approximately 5–25% and similar to the sampling precisions observed by *Doskey and Bialk* [2001] in a comparison of three sampling methods.

[11] The canister samples were analyzed using GC/FID combined with a cryogenic preconcentration approach [*Lonneman*, 1998]. The preconcentration procedure consists of a 6-port gas sample valve (Valco Model VIII, Houston, TX) in which the loop consists of a 20 cm × 0.32 cm o.d. stainless steel tube packed with 60–80 mesh untreated glass beads. In operation the tube, shaped as a loop, is immersed into a Dewar containing liquid argon (−187°C) and allowed to come to temperature equilibrium. A measured 300 mL aliquot of the canister sample air is passed through the loop trapping out the VOCs from the air. When trapping is complete the cryogen is removed and immediately replaced with another Dewar containing hot water (~99°C) and the trapped VOCs are routed to the GC column which is temperature programmed from −50° to 200°C at a rate of 8°C min^{-1}. Two GC columns were used for each sample analysis including a 60 m × 0.32 mm i.d. fused silica column coated with 1 μm polydimethylsiloxane (DB-1 J&W Scientific, Folsom, CA) for the C_2–C_{12} compounds, and a second column consisting of a similar 60 m ×

0.32 mm i.d. fused silica column with a thicker phase 3 μm polydimethylsiloxane to improve the resolution of the C_2-C_3 compounds. Both columns used identical temperature programming procedures. GC peak identification was determined by peak retention time using a CALTABLE developed with complex ambient air samples combined with known mixtures of VOCs. The FID calibration was performed using a National Institute of Standards (NIST) Standards Reference Material (SRM) propane in air standard (accuracy ±1.2%). Five distinct mixing ratios, achieved by dynamically diluting the SRM standard with ultra pure air were used to prepare the calibration curve. Precision for the lowest propane standard mixing ratio, i.e., 2.5 parts per billion C, was ±1.9%. The slope of the straight line obtained from the five standard samples provided a FID response factor in ppbC per peak area counts which was used for all GC peaks. The utilization of a single per carbon response factor for all GC peaks appears to be valid, particularly for hydrocarbon-type VOCs [*Leveque*, 1967; *Ackman*, 1968; *Blades*, 1976; *Apel et al.*, 1994], and is a typical practice for GC/FID applications. The accuracy provided with the NIST-SRM standard applies directly to the propane results in canister samples and it is expected that the accuracy of the other hydrocarbon-type VOCs to be reasonably similar. However, due to the complex composition of ambient air and the incomplete gas chromatographic resolution of many analytes, the analytic precision for coeluting VOCs could be as much as an order of magnitude larger than the precision of a completely resolved standard mixture [*Doskey and Bialk*, 2001].

2.3. Flight Path

[12] The aircraft measurements used in this study were made on 22 June 1999 between 2 PM and 3:30 PM central standard time (CST) at an approximately constant altitude of 700 m above the mean sea level (~550 m above the ground level). This sampling time was selected to coincide with the period when peak levels of O_3 are expected. The flight path consisted of two concentric circles of 9.25 and 18.5 km radii above the urban source region followed by a series of five ~70-km east-west transects at increasing downwind distances, extending up to ~60 km north of the Nashville downtown (Figure 1). The southern edge of the outer sampling circle abutted the edge of the greater Nashville metropolitan region while the western edge of the inner sampling circle was over the downtown area. Figure 1 also displays the locations of the hydrocarbon canister samples and the observed ozone mixing ratios along the flight path, showing a ozone plume north-northwest of Nashville, with values exceeding 110 ppb just downwind of the urban area, and a peak value of ~132 ppb along the third downwind transect.

3. Observations and Discussion

[13] The weather on 22 June was characterized by light southeasterly flow at 850 mb with high dew-points and sparsely scattered cumulus throughout the region. Figure 2 shows the vertical profiles of wind speed and direction and an estimate of the mixed layer height determined from a radar wind profiler at the Cornelia Fort site on 22 June between 9:30 and 15:30 CST (W. Angevine, personal communication, 2002). The change with time of the wind direction at 550 m suggests that a plume emanating from downtown would have traveled to the northwest until about 11:30 CST, and then shifted to the north-northeast of the city until the aircraft measurements were made that afternoon. This movement of the plume centerline is confirmed by the location of the peak values of NO_y, which we have used to define the plume centerline, shown as points C_0 through C_5 in Figure 3. It should be noted that although the plume center labeled C_5 in Figure 3 appears at the highest NO_y value encountered by the aircraft, it may not represent the actual plume centerline as the aircraft may have exited the plume prior to sampling the centerline. The corresponding back-trajectories, T_0 through T_5, for these points were calculated using the wind profiler measurements (Figure 3). The back-trajectories confirm that the sampling volume passed over the Nashville downtown area, near the Polk Building site. We will therefore use observations from this site to characterize the initial conditions for air parcels following these trajectories, and also define a "plume age" associated with the processing of this mix starting with its passage over the Polk Building. We will make extensive use of these features in the following analysis.

[14] Figure 4 shows a summary of the mean concentrations of O_3, NO_y, and NO_z measured along the plume centerline as a function of their estimated travel times from downtown. These means were calculated over ~5–6 km flight tracks at the centerline points. The simultaneous increases in O_3 and NO_z concentrations with plume age indicate photochemical production of O_3 and conversion of NO_x to HNO_3, PAN, organic nitrates (ONIT), and other nitrogen containing species that constitute NO_z. Although none of the PAN measurements (made only once every 7.5 min, as noted earlier) were made directly near the plume centerline, we make use of the fact that PAN and O_3 are highly correlated in aged urban plumes to obtain representative values of PAN by multiplying the PAN/O_3 ratio from the closest PAN observation by the average O_3 mixing ratios observed along the centerline. This approach suggests PAN concentrations range between 4.5 and 5.0 ppb along points C_2-C_5.

3.1. Observation-Based OPEs

[15] *Trainer et al.* [1993] found a linear relationship between O_3 and the concentration of NO_x oxidation products, NO_z, in photochemically aged air sampled at rural locations in the eastern U.S. and Canada, and showed that a measure of the ozone production efficiency could be estimated from the slope of the linear regression of O_3 versus NO_z. In the 1995 field campaign in Nashville [*Cowling et al.*, 1998], *Sillman et al.* [1998] and *St. John et al.* [1998] analyzed different urban O_3 episodes using this technique and found that the "regression OPE" varied between 4.0 and 6.5. Often $O_3 + NO_2$ (cumulatively referred to as 'O_x,' odd oxygen) is used in the regression analysis instead of O_3 because it tends to be more of a conserved quantity than O_3 in that it is not affected by the titration reaction, $NO + O_3 \rightarrow NO_2$ when NO_x is added to an air parcel [*St. John et al.*, 1998]. Figure 5 shows the plot of O_x versus NO_z for the observations shown in Figure 3. The slope of a linear least squares fit yields a regression OPE of 4.7 ± 0.2 (r^2 = 0.88,

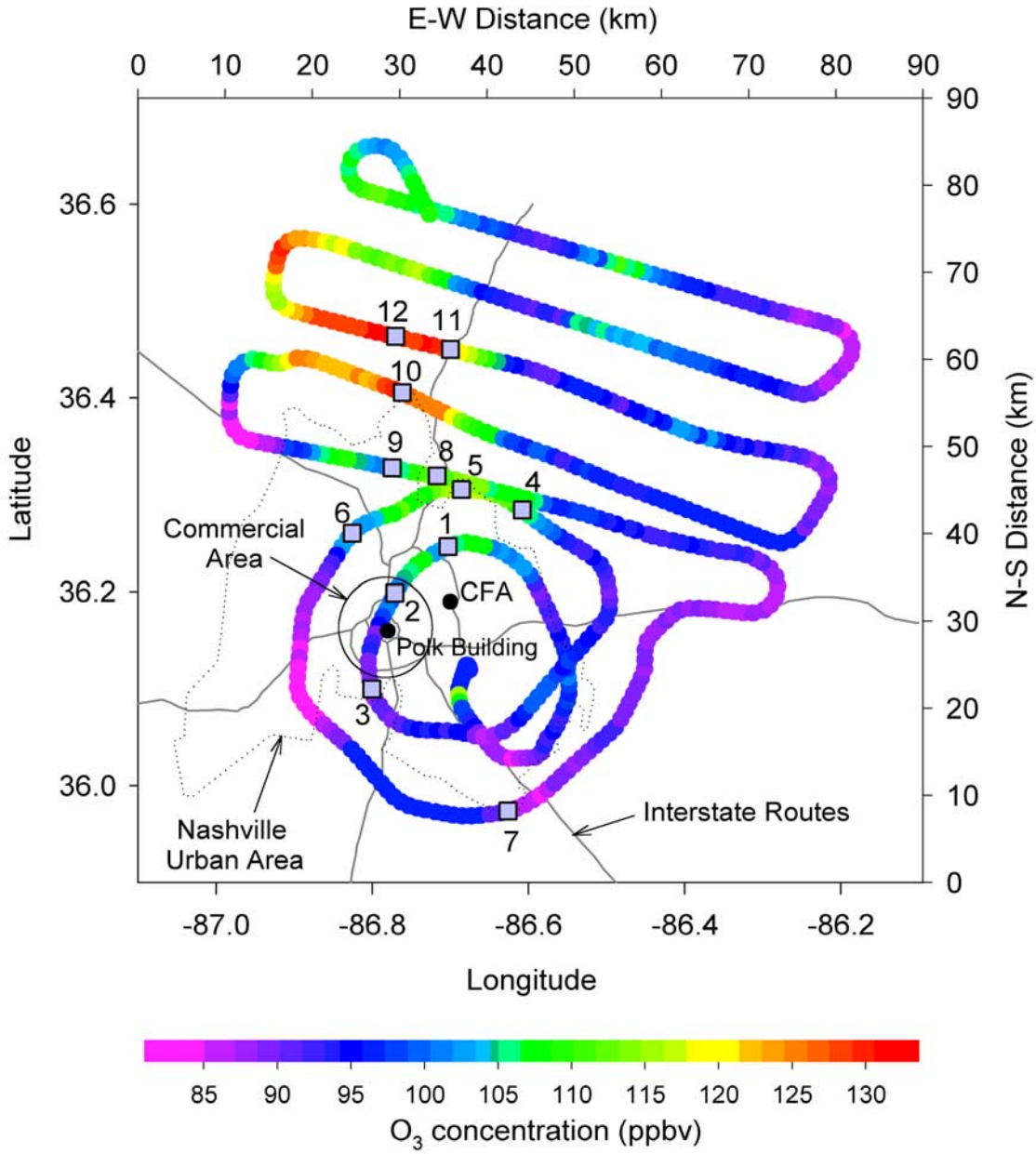

Figure 1. Ozone concentrations based on 10 s average measurements made along the flight path to show the location of the urban plume. Also shown are the locations of the VOC canister samples (numbered gray squares) along the flight path, and the two ground sites: Cornelia Fort Airpark (CFA) and Polk Building. The dotted line represents the boundary of the Nashville urban area; the gray lines indicate the interstate routes; and the circle around the Polk Building approximately shows the extent of the commercial area surrounding the downtown.

and the uncertainty estimate is for a level of confidence of approximately 95%) for this plume, consistent with previous studies [*St. John et al.*, 1998; *Nunnermacker et al.*, 1998]. Uncertainty in the regression OPE due to measurement errors in O_x and NO_z is estimated at approximately ±25%, which translates into a value of 4.7 ± 1.2.

[16] However, interpretation of regression OPE is often problematic, because it contains observations from different air parcels of different photochemical ages and histories in which O_3 has been produced under a variety of conditions [*Trainer et al.*, 2000]. Since O_3 is produced more efficiently at low-NO_x levels and vice versa, and given that the relation between the net OPE and NO_x concentrations is highly nonlinear, it is not clear why there is usually a strong correlation between O_x and NO_z [*Kleinman et al.*, 2002]. Nevertheless, the regression OPE characterizes the reactivities of different air parcels of different photochemical ages and emission histories by a single statistic, which makes it difficult to apply in formulating regulatory strategies.

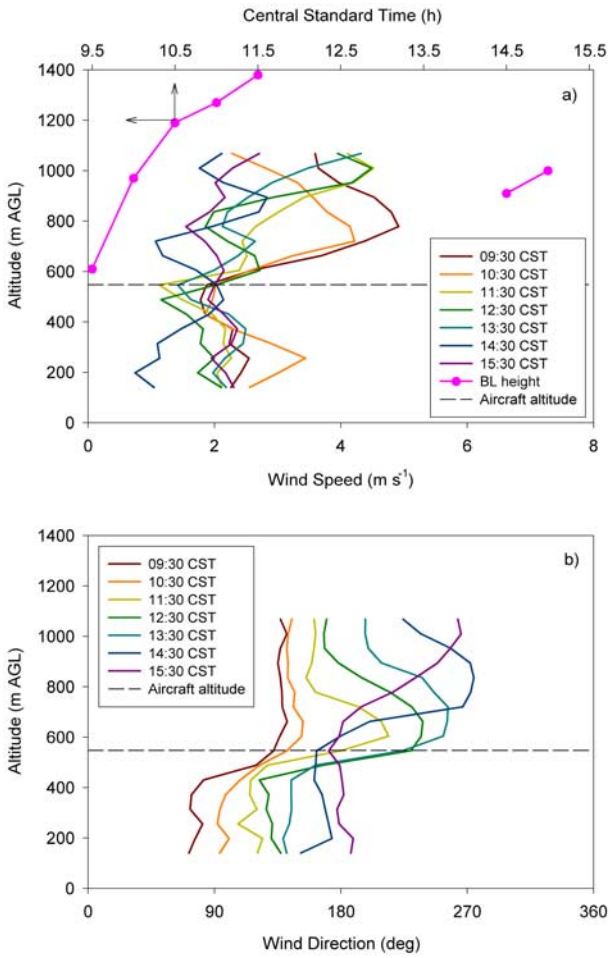

Figure 2. Wind profiler data measured at CFA: (a) hourly vertical wind speed profiles and boundary layer height along with the aircraft flying altitude; (b) vertical wind direction profiles. The G-1 flight time was from 14:00 to 15:30 CST.

[17] To illustrate the above point, we estimate cross-plume OPEs along the plume centerline points, C_1–C_5, as the ratio of excess O_x to excess NO_z at the plume center relative to conditions at the edge of the plume along a crosswind transect

$$\text{Cross}-\text{plume OPE}(t) = \frac{[O_x(t)]_{\text{plume center}} - [O_x(t)]_{\text{plume edge}}}{[NO_z(t)]_{\text{plume center}} - [NO_z(t)]_{\text{plume edge}}}, \quad (1)$$

where t is time. The plume edge points (E_1–E_5) needed for calculating the cross-plume OPEs are defined along the crosswind transects perpendicular to the back-trajectories at the downwind centerline points (Figure 6a). The resulting cross-plume OPEs are shown in Figure 6b as a function of the air parcel age, i.e., the estimated travel time from the downtown area. With this definition, the cross-plume OPE is found to increase from ~2.0 at C_1 to 5.6 at C_4, clearly showing that O_3 was produced more efficiently as the air parcel aged. This trend in cross-plume OPE for an urban plume qualitatively agrees with the net OPE estimated by *Ryerson et al.* [1998, 2001] and *Sillman* [2000] in power plant plume air parcels as a function of air parcel age. It should be noted that they used different approaches based on the mass fluxes of O_3 and NO_x through plume cross sections at increasing downwind distances; however, within the associated uncertainties, these approaches should give quantitatively similar results.

[18] However, because O_3 observed in the afternoon in the urban air parcels at C_1–C_5 was formed over different time periods of the day, with different emissions of NO_x and VOCs along its different trajectories, the cross-plume OPEs shown in Figure 6b do not reveal how the OPE changed in each individual Lagrangian air parcel as a function of time. To quantify the net efficiency of O_3 production in an air parcel as it travels downwind of an urban source region, one must evaluate the "Lagrangian OPE." In the discussions to follow, it will be useful to distinguish two perspectives of Lagrangian OPE: instantaneous and cumulative. The "instantaneous Lagrangian OPE" is a function only of the local rates of production and destruction of O_3 and NO_x due to chemistry and dry deposition while the "cumulative Lagrangian OPE" represents an integrated value in reference to an arbitrarily chosen starting point. Observations of O_x and NO_z can be used to provide an estimate of the cumulative Lagrangian OPE if the measurements in an identified parcel of air are available when it leaves its source region (at initial time t_0) and again later when this same parcel has undergone chemical processing (at any time t):

$$\text{Observed Cumulative Lagrangian OPE}(t) = \frac{[O_x(t)] - [O_x(t_0)]}{[NO_z(t)] - [NO_z(t_0)]} = \frac{\Delta[O_x(t)]_{\text{obs}}}{\Delta[NO_z(t)]_{\text{obs}}}. \quad (2)$$

However, this as well as the regression and cross-plume methods described above, tend to overpredict the OPE, unless they take into account the NO_z losses due to dry deposition. Their interpretation is also complicated by other processes such as dilution, cloud-venting, and fresh emissions in an air parcel as it moves downwind. In the absence of continuous observations of O_3 production, NO_x destruction, dry deposition rates, emissions, and mixing within a specific air parcel, the Lagrangian OPEs within a parcel of air must be evaluated using a numerical model that includes mathematical representations of these processes. A model to evaluate these OPEs is described in the following section.

4. Model Analysis

4.1. The Model

[19] We use a zero-dimensional Lagrangian box model that includes photochemical reactions, dry deposition, and allows for horizontal dilution and vertical entrainment in a developing boundary layer, as described by:

$$\frac{dC_i}{dt} = R_i - \frac{v_{d,i}}{H(t)}C_i + \frac{E_i(t)}{H(t)} - \lambda(C_i - C_{i,b}) \quad \text{for} \quad \frac{dH}{dt} \le 0, \quad (3)$$

$$\frac{dC_i}{dt} = R_i - \frac{v_{d,i}}{H(t)}C_i + \frac{E_i(t)}{H(t)} - \lambda(C_i - C_{i,b}) + \frac{(C_{i,a} - C_i)}{H(t)}\frac{dH}{dt} \quad \text{for} \quad \frac{dH}{dt} > 0, \quad (4)$$

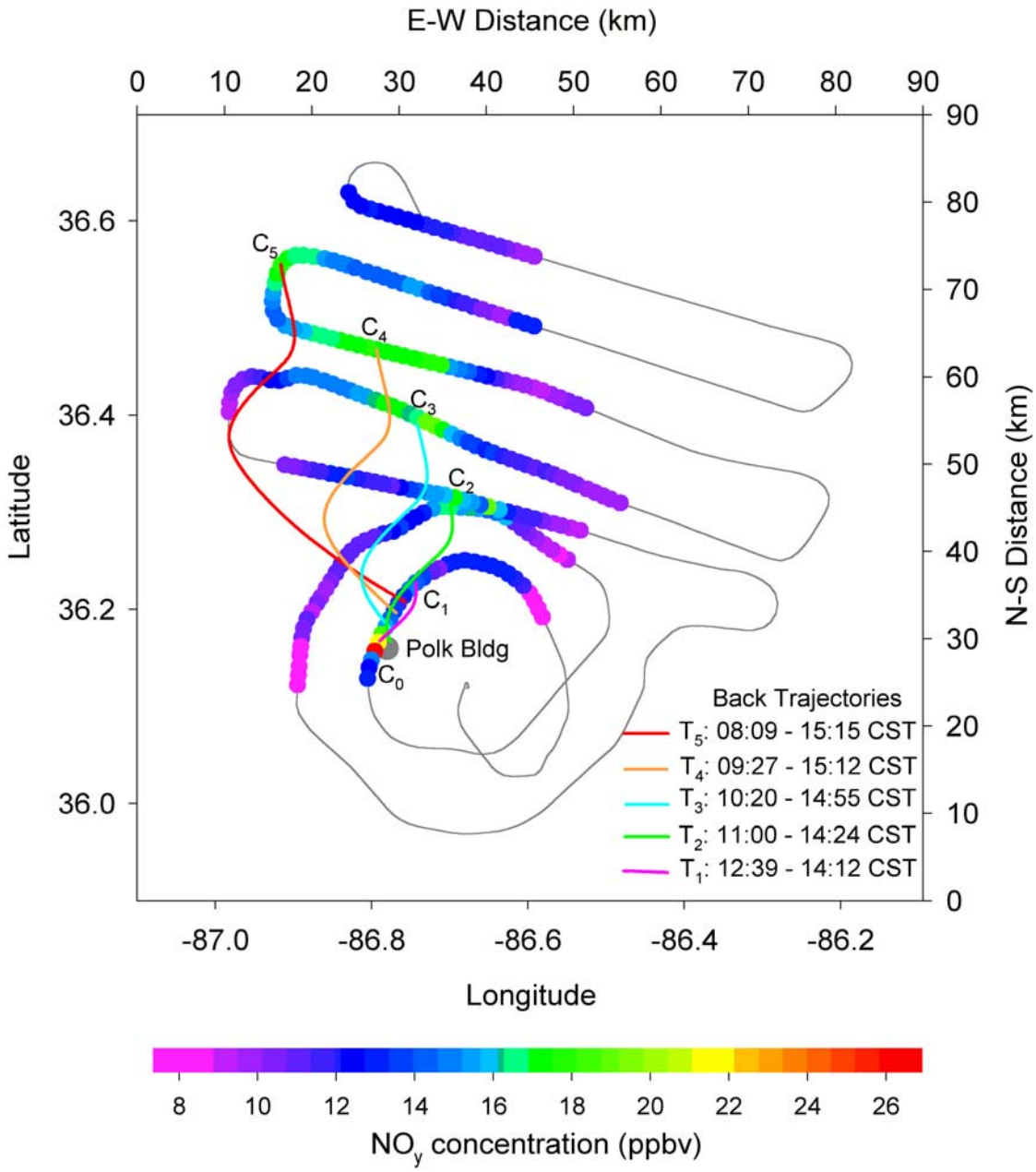

Figure 3. NO_y concentrations along the flight path. Centerline points are marked C_0 through C_5 at peak concentrations and back trajectories from these points are calculated using the wind profiler data (see text).

with the initial condition for the solution as:

$$C_i(0) = C_i^0. \tag{5}$$

Here C_i is the average concentration (molecule cm^{-3}) of species i in the urban plume; $C_{i,b}$ is the background concentration of species i; $C_{i,a}$ is the concentration aloft, above the mixed layer; C_i^0 is the initial concentration of the species i; R_i is the net rate (molecule cm^{-3} s^{-1}) of chemical reaction of species i; $v_{d,i}$ is the dry deposition velocity (cm s^{-1}) of species i; $E_i(t)$ is the emission rate (molecule cm^{-2} s^{-1}) of species i at time t; $H(t)$ is the height (cm) of the mixed layer at time t; and λ is a first-order dilution rate parameter (s^{-1}). Conceptually, the box extends vertically to $H(t)$ while its horizontal dimensions are selected arbitrarily, and all species are assumed to be well mixed within this box. Here we assume the base of box to be 12 km $\times$ 12 km, which corresponds to the downtown Nashville and its surrounding commercial area. Although equations (3) and (4) do not explicitly contain the horizontal dimensions, the size of base of the box is needed for averaging the observed concentrations over its area for evaluating the model since C_i is defined as average concentration in the box. This box, which represents an urban air parcel, is allowed to move with the wind in an air-shed as it collects emissions of trace gases, which undergo chemical reactions and dry deposi-

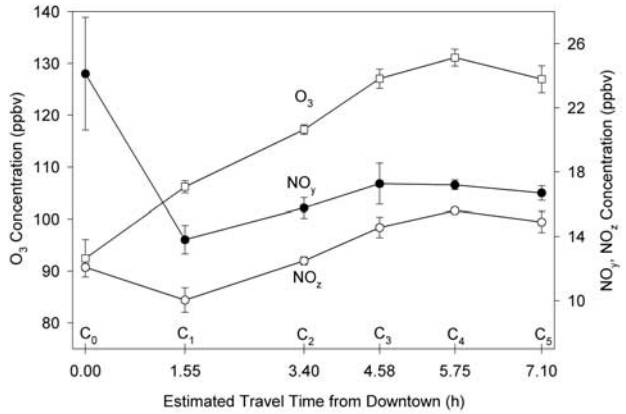

Figure 4. Mean centerline concentrations of O_3, NO_y, and NO_z plotted as a function of the estimated travel time of the different air parcels from the Nashville downtown area. The means were calculated over 5–6 km flight-tracks at the centerline, and the vertical error bars represent one standard deviation. The lines connecting the data points are guides for the eye.

tion. The wind profiles shown in Figure 2 suggest that plume of 22 June would have undergone significant dispersion due to directional wind shear, with subsequent vertical mixing within the boundary layer causing dilution of the plume with the background air. This phenomenon is represented by the dilution term $\lambda(C_i - C_{i,b})$ in equations (3) and (4), where λ is simply a model construct that lumps the rates of the complex processes described above into one parameter (quantified in subsection 4.3). Since fair-weather cumulus were sparsely scattered in the region of interest, dilution due to cloud-venting at the top of the model domain has been neglected.

[20] The gas-phase chemistry is modeled with the photochemical mechanism CBM-Z [*Zaveri and Peters*, 1999]. CBM-Z employs the lumped-structure approach for condensing organic species and reactions, and is based on the widely used Carbon Bond Mechanism (CBM-IV) developed by *Gery et al.* [1989] for use in urban air-shed models. CBM-Z contains 53 species and 133 reactions, and includes revised inorganic chemistry; explicit treatment of lesser reactive paraffins such as methane and ethane; revised parameterizations of the reactive paraffins, olefins, and aromatic reactions; alkyl and acyl peroxy radical interactions and their reactions with the NO_3 radical; longer-lived organic nitrates and hydroperoxides; and revised isoprene chemistry based on the condensed one-product mechanism of *Carter* [1996]. The version of CBM-Z used here contains an additional lumped species "ANOL," which represents ethanol and higher alcohols. ANOL reacts with the OH radical to produce an ALD2 (lumped aldehyde species) and an HO_2 radical.

4.2. Model-Based Lagrangian OPEs

[21] The instantaneous Lagrangian OPE can be obtained from the above model as:

$$\text{Instantaneous Lagrangian OPE}(t) = \frac{(d[\mathrm{O_3}(t)]/dt)_{\text{chem+dry dep}}}{-(d[\mathrm{NO}_x(t)]/dt)_{\text{chem+dry dep}}}, \tag{6}$$

where the numerator and denominator are the instantaneous rates of changes of O_3 and NO_x concentrations, respectively, in an air parcel due only to photochemistry and dry

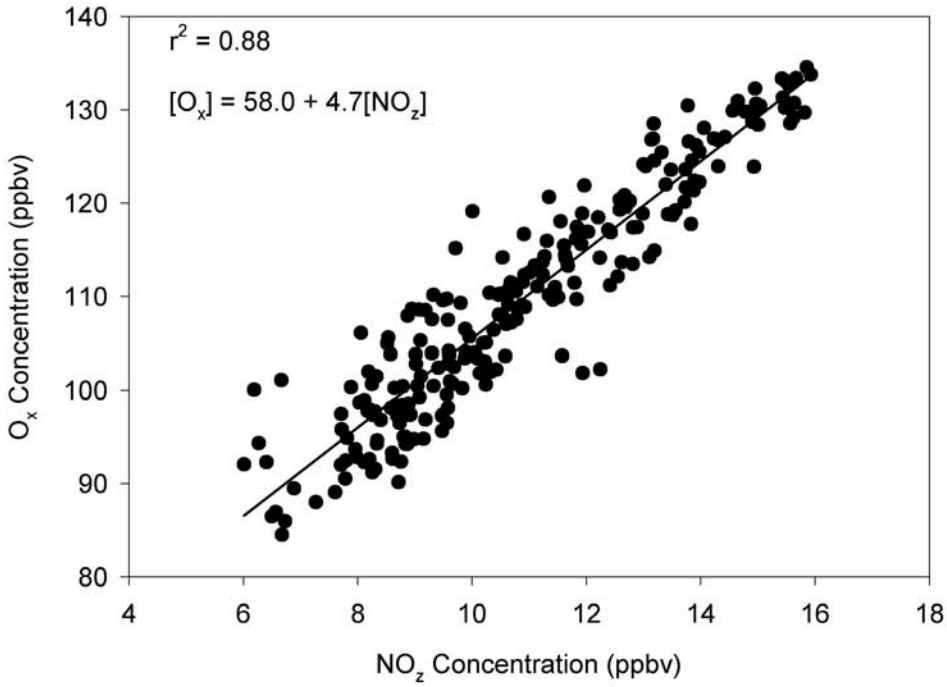

Figure 5. Scatter plot of odd oxygen O_x (= O_3 + NO_2) and NO_z for the sample points shown in Figure 3, with a least squares linear fit giving a "regression" OPE = 4.7.

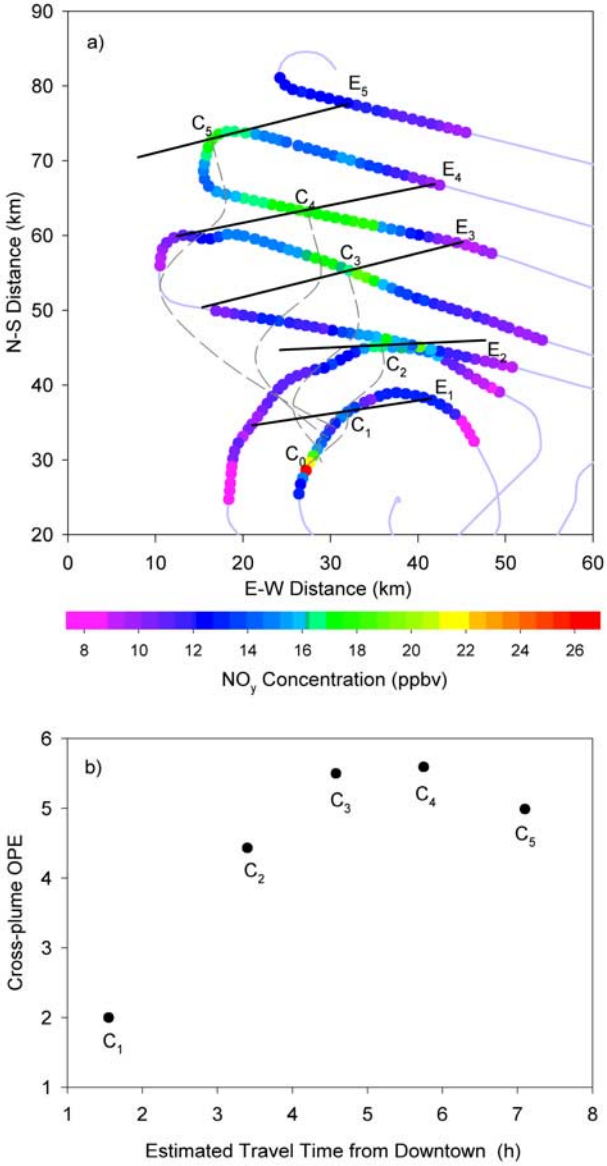

Figure 6. (a) Plume edge points (E_1–E_5) marked along the crosswind sections across the centerline points; (b) cross-plume OPE plotted at these cross sections as a function of the estimated travel time of the air parcels from the downtown area.

deposition at a given time. Similarly, the cumulative Lagrangian OPE can be calculated as:

$$\text{Cumulative Lagrangian OPE}(t) = \frac{\Delta[O_3(t)]_{\text{chem+dry dep}}}{-\Delta[NO_x(t)]_{\text{chem+dry dep}}}, \quad (7)$$

where the numerator and denominator are the integrated net changes in the O_3 and NO_x concentrations, respectively, in a parcel of air due only to photochemistry and dry deposition from when it was just upwind of an arbitrary starting point ($t = 0$). It should be noted that both the definitions still allow for the indirect effects of fresh emissions and plume dilution. In other words, fresh emissions and plume dilution terms are included in the model simulation, but are not included in the calculation of $\Delta[O_3]$ and $\Delta[NO_z]$. The Δ values are determined by integrating the concentration changes as a function of time due to just chemistry and dry deposition terms in equations (3) or (4).

[22] Furthermore, it would also be useful to know the net number of O_3 molecules photochemically produced in an air parcel for every molecule of NO_x lost due to photochemistry only. We call this quantity the net "chemical OPE." The instantaneous and cumulative chemical OPEs are same as their Lagrangian counterparts, but exclude the dry deposition term:

$$\text{Instantaneous Chemical OPE}(t) = \frac{(d[O_3(t)]/dt)_{\text{chem}}}{-(d[NO_x(t)]/dt)_{\text{chem}}}, \quad (8)$$

$$\text{Cumulative Chemical OPE}(t) = \frac{\Delta[O_3(t)]_{\text{chem}}}{-\Delta[NO_x(t)]_{\text{chem}}}. \quad (9)$$

Not including dry deposition of NO_x makes the denominator smaller and therefore the chemical OPEs larger than Lagrangian OPEs; but an even bigger effect is due to the neglect of dry deposition of O_3, which has a higher deposition velocity than NO and NO_2. Both the effects act in the same direction to make the chemical OPEs larger than the corresponding Lagrangian OPEs, thus serving as their upper limits. Again, it should be noted that the chemical OPEs contain the indirect effects of dry deposition, fresh emissions, and plume dilution, which are present in the simulation, but are excluded only while computing the OPEs. The chemical OPEs therefore represent the maximum net efficiency with which O_3 can be produced in an air parcel for a given set of initial concentrations, fresh emissions, dilution, and other factors such as temperature and solar actinic flux.

4.3. Model Scenario and Inputs

[23] No direct observations are available to characterize the upper air early morning, initial conditions within the air parcels that were subsequently sampled downwind of Nashville during the afternoon flight of 22 June. However, observations made during the 1995 Nashville campaign [*Berkowitz and Shaw*, 1997; *Luke et al.*, 1998] suggest these upper air values can be evaluated from measurements made at the surface in a well-mixed boundary layer. During this earlier Nashville campaign, *Berkowitz and Shaw* [1997] compared aircraft and surface observations at a rural site under clear skies and light winds during the morning transition from nocturnal stable stratification to the afternoon convective mixed layer. They found that surface ozone values steadily increased in time until they matched the values aloft by midmorning as a result of the downward mixing of air aloft. In a similar study, *Luke et al.* [1998] found modest horizontal and vertical gradients in O_3, CO, NO_y, and SO_2 concentrations over the Nashville downtown area, suggesting that these species were uniformly mixed in the fully developed boundary layer.

[24] Evidence that this phenomenon occurred on the morning of 22 June 1999 can be seen in the measurements

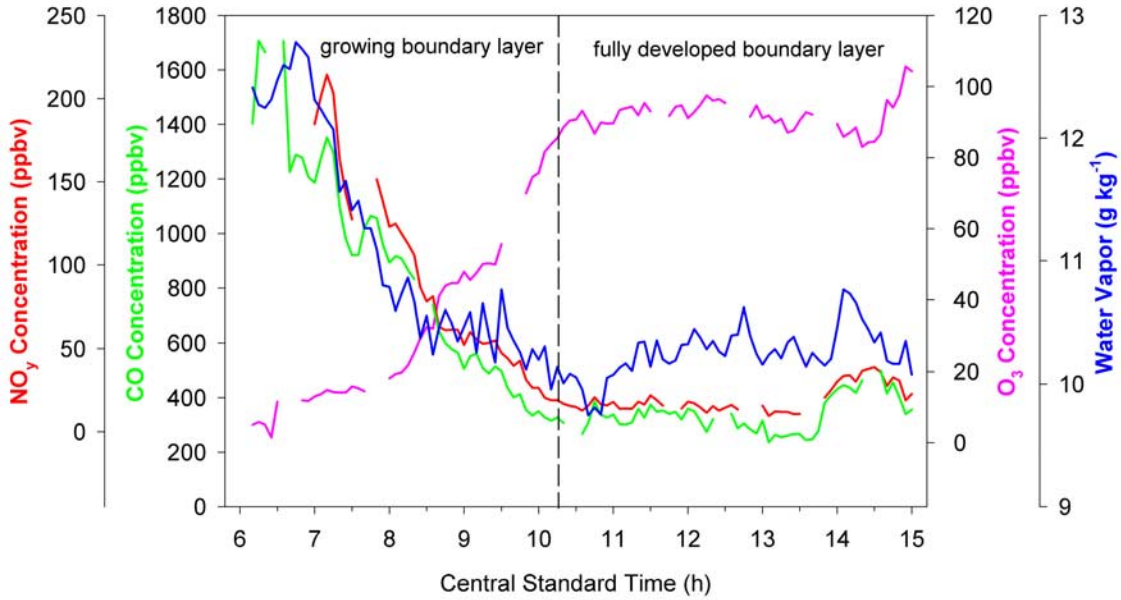

Figure 7. Evolution of trace gases atop Polk Building. The vertical dashed line marks the time when the growing boundary layer is fully developed.

of O_3, NO_y, CO, and water vapor (Figure 7) made atop the Polk Building [*Olszyna*, 2002]. Prior to approximately 10:15 CST, all of these quantities were changing. Ozone concentration increased from a few ppb to 90 ppb and then remained relatively constant. CO, water vapor, and NO_y mixing ratios all decreased until this time, and then remained relatively constant. We assume that the trends observed at the Polk Building on the morning of 22 June 1999 result from the similar mixing process seen during the 1995 Nashville campaign. Prior to ~7:30 CST, the surface air was decoupled from the air aloft resulting in high concentration of species having a nocturnal source at the surface, e.g., CO, NO_y, and water vapor. With the onset of convective mixing after sunrise, these species were diluted at a common rate while high O_3 concentration in the residual layer aloft was brought to the surface. As noted in the work of *Berkowitz and Shaw* [1997], the volume of air trapped by the relatively shallow nocturnal boundary layer would have a smaller effect on the final mixing ratios relative to the deeper column of air aloft being mixed to the surface. The mixed layer height at ~10:15 CST reached ~1200 m AGL and is assumed to have remained relatively constant thereafter.

[25] This simple conceptual model in conjunction with the observations from the Polk Building suggest that the air over Nashville was within a fully developed mixed layer after about 10:15 CST. We therefore used 10-min average values of O_3, NO_x, NO_z (= $NO_y - NO_x$), and CO from the Polk Building to initialize the box model simulation for the air parcel trajectory T_3 (shown in Figure 3) that began at 10:20 CST. The initial VOC concentrations used for this model scenario came from the Polk Building canister sample taken at 11:00 CST. Background concentrations of NO_x, NO_z, O_3, CO, and VOCs were assumed to stay steady at the average levels observed by the G-1 at the edge of the plume. Both initial and background concentrations are summarized in Table 1.

[26] While both the initial and background NO_z concentrations are estimated at 8.2 ppb, their compositions are not readily apparent. PAN concentration in aged background air would be in thermal equilibrium with NO_2 and acyl peroxy radical. A simulation for the background conditions, in which the NO_x and VOC concentrations are held steady, predicts that the PAN concentrations would need to be ~2.0 ppb (at 297 K) for it to also remain constant. Both initial and background PAN concentrations are therefore set to 2.0 ppb. Initial and background ONIT concentrations are assumed at 0.2 ppb, while the remaining 6.0 ppb NO_z is assumed as HNO_3.

[27] Typical daytime values of dry deposition velocities for key species are also listed in Table 1 and were held constant during the simulation, as were temperature, pressure, and relative humidity at 297 K, 940 mb, and 57%, respectively. The average dry deposition velocity for nitric acid of 3.0 cm s^{-1} is based on the estimated values reported for the U.S. EPA CASTNET sites in rural Tennessee for the month of June between 10:00 and 15:00 CST (these data are available on the internet at http://www.epa.gov/castnet/data.html). The dry deposition velocity for H_2O_2 of 2.0 cm s^{-1} is adopted from *Jobson et al.* [1998] while all other values are taken from *Duncan and Chameides* [1998]. Although the mixed layer height appears to have varied between 1000 and 1400 m during the period of interest, for simplicity we have used a representative value of 1200 m, thereby allowing the use of equation (3) in which $dH/dt \leq 0$.

[28] Hourly emission rates of 15 CBM-Z species at 4-km resolution were obtained from the Sparse Matrix Operator Kernel Emissions (SMOKE) processor [*Houyoux et al.*, 2000]. For this study, the emissions were based on the meteorology from the RAMS [*Pielke et al.*, 1992] simulation for a typical summer weekday period for the Nashville area. Figure 8 shows the spatial distribution of the NO_x emissions at 10:00 CST. Also shown are the locations of the

Table 1. List of Initial and Background Concentrations and Dry Deposition Velocities

Species Symbol	Initial Concentration C_i^0, ppbv	Background[a] $C_{i,b}$, ppbv	$v_{d,i}$,[b] cm s^{-1}	Species Name
		Inorganic and NO_y Species		
Source	Polk Building	Plume Edge[c]		
O_3	90.0	95.0	0.8	ozone
CO	300.3	150.0	0.03	carbon monoxide
H_2O_2	1.0[d]	1.0[d]	2.0	hydrogen peroxide
NO_y	17.2	9.3	...	total reactive nitrogen
NO_2	7.7	1.0	0.4	nitrogen dioxide
NO	1.3	0.1	0.016	nitric oxide
NO_z	8.2	8.2	...	$NO_y - (NO_2 + NO)$
HNO_3	6.0[d]	6.0[d]	3.0	nitric acid
PANs	2.0[b]	2.0[b]	0.4	peroxyacyl nitrates
ONIT	0.2[d]	0.2[d]	0.1	organic nitrate
		Hydrocarbon Species		
Source	Canister at 11 CST	Canister 6		
CH_4	1700.0[d]	1700.0[d]	...	methane
C_2H_6	3.0	2.9	...	ethane
PAR	43.7	15.1	...	paraffins
CH_3OH	5.7	5.6	...	methanol
ANOL	4.2	0.3	...	alcohols
HCHO[e]	6.0 ± 0.5	6.0	...	formaldehyde
ALD2	2.6	1.5	...	aldehydes
AONE	4.3	3.8	...	ketones
ETH	0.74	0.20	...	ethane
OLET	0.42	0.09	...	terminal olefins
OLEI	0.21	0.09	...	internal olefins
TOL	1.51	0.71	...	toluenes + benzenes
XYL	1.53	0.13	...	xylenes
ISOP	0.08	0.10	...	isoprene

[a]Background concentrations were derived from aircraft observations.
[b]See text.
[c]Plume edge concentrations are averages of values at points E_2 to E_4 in Figure 6a.
[d]Assumed.
[e]HCHO was measured at the CFA site (A. Fried, personal communication, 2003).

two surface sites and the air parcel trajectory T_3. Positions of the air parcel along T_3 at every hour starting at 10:00 CST were calculated, and the nearest emission grid points to these positions within a radius of 6 km were used to determine the hourly average emissions for each species. The resulting values were then temporally interpolated using cubic splines to produce 1-min emission inventories for the Lagrangian air parcel.

[29] Photolysis frequencies in the Lagrangian box model were based on surface values determined at the CFA site during the field campaign using actinic flux spectroradiometry [*Shetter et al.*, 2003]. While clouds were present in the region, and these affected local J values, they were very sparse and highly scattered. Photolysis rates increase with altitude due to surface albedo as well as backscattering of incoming solar radiation by air molecules and aerosols. Although these effects depend on the wavelength, we assumed an average 15% enhancement in the photolysis rates for the entire mixed layer depth over the surface values based on the vertical profiles of J_{NO_2} computed using the radiative transfer code Fast-J [*Wild et al.*, 2000]. Emissions of NO_x, formaldehyde (HCHO), and isoprene, and J_{NO2} values as a function of time are shown in Figure 9 as examples to illustrate the estimated changing emissions and radiation environment the air parcel experienced as it was advected along the trajectory T_3.

[30] Last, the dilution rate parameter, λ, was estimated from the rate at which the urban plume broadened downwind of the downtown area. Assuming there is negligible dispersion in the direction of advection, we can define λ as the fractional rate at which the vertical cross-sectional area (A) of the plume increases with time:

$$\lambda = \frac{1}{A}\frac{dA}{dt} = \frac{d\ \ln A}{dt} = \frac{\Delta \ln A}{\Delta t} = \frac{\Delta \ln(W \times H)}{\Delta t}, \qquad (10)$$

where W and H are the plume width and height, respectively. Furthermore, assuming that the plume remained confined within the mixed layer of constant height, equation (10) reduces to

$$\lambda = \frac{\ln\left(W_f/W_i\right)}{\Delta t}, \qquad (11)$$

where W_f and W_i are the final and initial plume widths, respectively, and Δt is the transit time. Based on the spatial distribution of NO_x emissions in the downtown area (Figure 8), the initial plume width at C_0 is estimated to be ~12 km, which is also the width of the Lagrangian box. The final width of the plume is estimated to be about 20 km based on the spatial distribution of the observed NO_y concentrations in the plume across C_3, relative to the background values (Figure 6). A transit time of 4.58 hours for C_3 (Figure 4) yields a mean value of $\lambda = 3.1 \times 10^{-5}$ s^{-1}.

[31] The resulting system of nonlinear ordinary differential equations described by equation (3) was solved using LSODES, a GEAR-type solver [*Hindmarsh*, 1983]. A time step of 1 min was used to update the photolysis rate

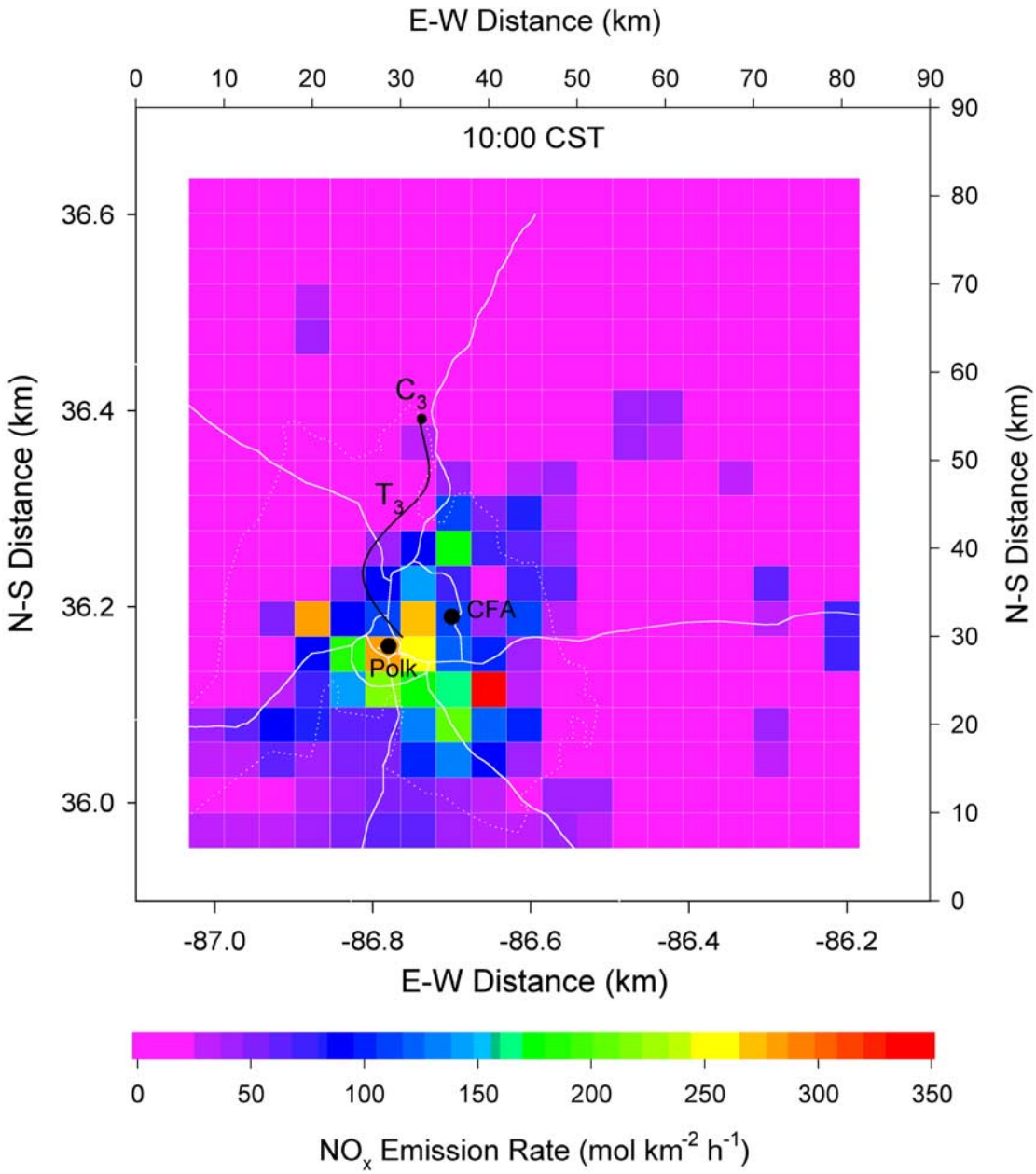

Figure 8. NO_x emission inventory from SMOKE processor at 4-km resolution along with back trajectory T_3.

coefficients and the emission rates. Instantaneous values of the species concentrations were also output every minute.

4.4. Model Evaluation and Discussion

[32] During the analysis of preliminary model results, we found that the simulated CO concentration was much larger than the observed CO levels at C_3. CO has a relatively long chemical lifetime (>6 days) and behaves as a conserved urban tracer for short time periods. It therefore serves as an important independent check for model performance. Linear regression of CO versus NO_x emission rates (from the SMOKE processor) along T_3 revealed that the CO emissions are approximately 10 times the NO_x emission rates, almost a factor of 1.6 higher than the emissions ratio of 6.3 ± 0.9 derived from measurements in Nashville in 1999 by *Parrish et al.* [2002]. We estimated a value of 5.0 ± 0.3 for the CO/NO_x emissions ratio from the slope of the correlation of CO and NO_y concentrations observed at the Polk Building site on 22 June by restricting the data to the early morning rush hour (6:00–7:30 CST) when the observed NO_x/NO_y concentration ratio was greater than or equal to 0.99 (see Appendix A for the derivation of the relationship between the emission rates of CO and NO_x in terms of their ambient concentrations). For these reasons, we multiplied the SMOKE NO_x emissions rate by the empirically derived emissions ratio of 5.0 to obtain the model input emissions of CO.

[33] With these initial conditions and input values, the model not only predicted the CO concentration close to the

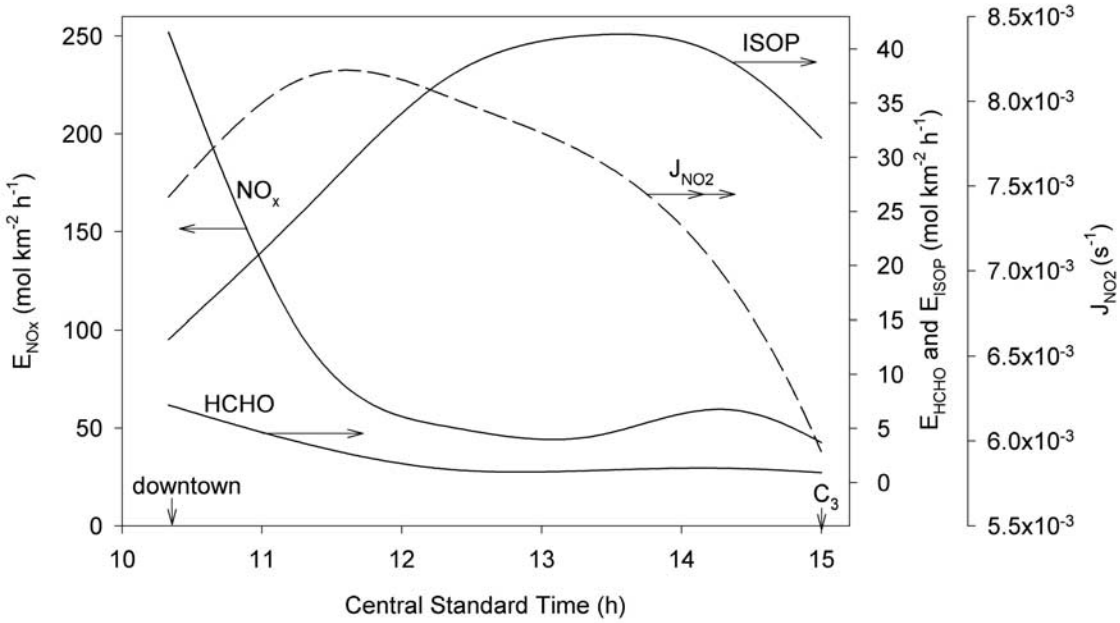

Figure 9. Examples of NO_x, HCHO, and ISOP emission rates along T_3 and smoothed clear-sky photolysis rate coefficient for NO_2 as a function of time.

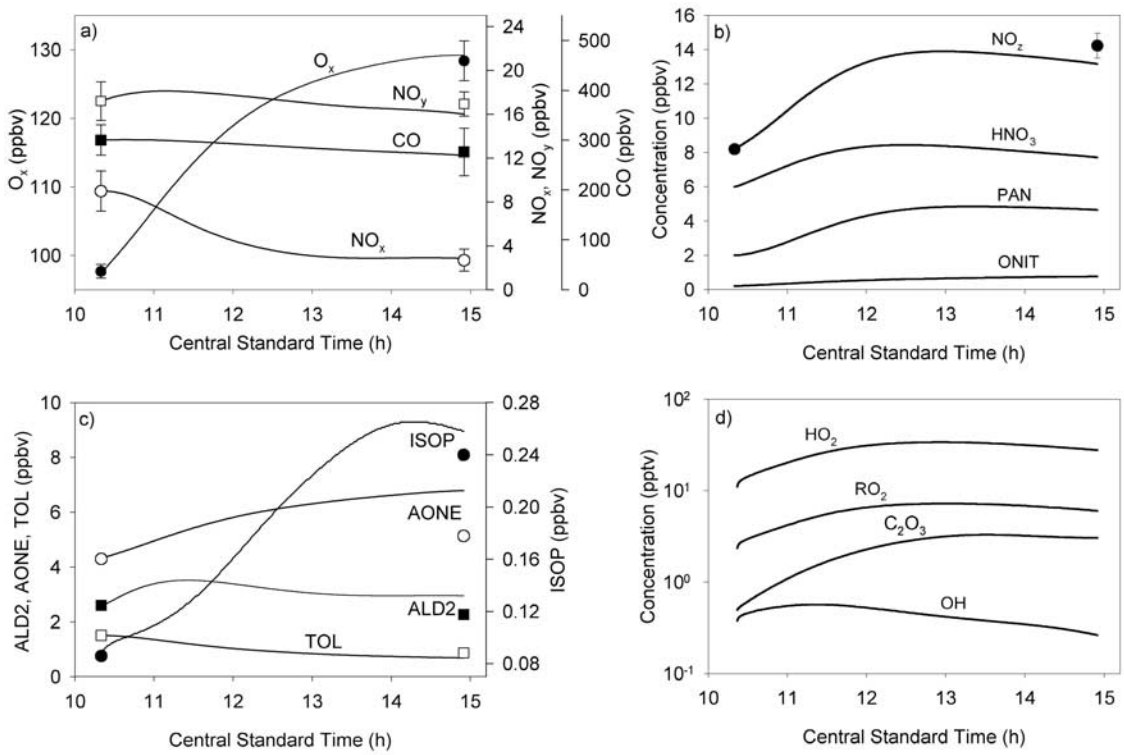

Figure 10. Simulated (lines) and observed (symbols) concentrations of some important trace species along T_3. Observations at the start of the simulation (at 10:20 CST) were made at the Polk Building and those at the end (at ~15:00 CST) were made by the G-1 aircraft. The vertical error bars on some of the observed mean concentrations represent one standard deviation (σ). (a) O_x, NO_y, and NO_x; (b) NO_z, PAN, ONIT, and HNO_3; (c) VOCs: AONE, ALD2, TOL, and ISOP; (d) radicals: HO_2 (hydroperoxy radical), RO_2 (lumped alkyl peroxy radical), C_2O_3 (peroxyacyl radical), and OH (hydroxyl radical).

Table 2. Comparison of Simulated and Observed Concentrations of Key Species at C_3

Species	Observed[a] at C_3, ppbv	Simulated at C_3, ppbv	
	Mean ± σ	$\lambda = 3.1 \times 10^{-5}\ s^{-1}$	$\lambda = 0.0\ s^{-1}$
O_3	126.0 ± 2.8	126.6	142.4
O_x	128.4 ± 2.9	129.2	145.5
CO	276.4 ± 47.5	269.6	340.0
H_2O_2	. . .	1.8	1.9
NO_y	16.9 ± 1.1	16.0	19.7
NO_2	2.4 ± 0.9	2.6	3.2
NO	0.34 ± 0.12	0.26	0.28
NO_z	14.2 ± 0.7	13.2	16.3
HNO_3	. . .	7.7	9.1
PAN	5.0	4.6	6.1
ONIT	. . .	0.7	1.0
Hydrocarbons	Canister 10		
C_2H_6	3.4	3.6	4.0
PAR	20.1	31.7	41.8
CH_3OH	12.2	5.2	5.0
ANOL	1.2	2.1	3.3
HCHO	. . .	5.7	6.1
ALD2	2.3	2.9	3.6
AONE	5.1	6.8	8.3
ETH	0.30	0.37	0.45
OLET	0.081	0.086	0.085
OLEI	0.086	0.081	0.075
TOL	0.87	0.68	0.75
XYL	0.11	0.10	0.10
ISOP	0.24	0.26	0.26

[a]Measurements made by the G-1 aircraft at ~15:00 CST.

observed mean (Figure 10), but also reproduced the observed mean NO_y concentration, both of which include the estimated effects of fresh emissions, dilution, and dry deposition. We also see excellent agreement between the simulated and observed O_x, NO_x, and total NO_z concentrations. It should be noted here that the observed concentrations were averaged over a distance of approximately 12 km flight path along the crosswind transect at C_3 for consistent comparison with the box-model mean concentrations.

[34] Since O_3 chemistry depends on both NO_x and VOCs, it is important to include comparisons of simulated and observed VOC species in the model evaluation. Canister 10, which is closest to C_3, is used to evaluate the simulated VOCs. However, since the VOCs in CBM-Z are lumped-structure species, the measured VOC concentrations measured were also converted into lumped species to allow direct comparisons. Some of the key VOC species plotted in Figure 10 show very good agreement between simulation and observations. Rerunning this base case scenario with the dilution turned off increased the predicted NO_y, CO, and O_3 at point C_3 by about 23, 26, and 12%, respectively. This indicates that the impact of plume dilution due to directional wind shear on downwind concentrations of O_3 and other species is quite significant, at least in this case, and cannot be ignored. The key results are summarized in Table 2. Although many assumptions and uncertainties exist in constraining the model, excellent agreement between the simulated and measured concentrations of a variety of key species strongly suggests that this model scenario does well in characterizing the chemistry and dynamics experienced by the air parcel at C_3 since leaving the Nashville downtown area. For this reason, we feel justified in using it to isolate photochemical O_3 production and NO_x oxidation from depositional loss, and to estimate the associated Lagrangian OPEs that this air parcel experienced as it was advected from the downtown area up to C_3.

[35] Figure 11a shows the instantaneous chemical production rate of O_3 (ppb h^{-1}) and the oxidation rate of NO_x along with the O_3 and NO_x dry deposition rates as a function of downwind processing time, within the air parcel following the trajectory T_3. The calculated NO_x oxidation rate increased from an initial ~3.0 ppb h^{-1} (~35% h^{-1}) to its peak value of about 4.6 ppb h^{-1} (~60% h^{-1}) by 11:00 CST, followed by a gradual decrease to ~0.7 ppb h^{-1} (~25% h^{-1}) by the time the air parcel reached C_3. The calculated chemical O_3 production rate displayed a similar shape, increasing from an initial ~14 ppb h^{-1} to a peak value of ~20 ppb h^{-1} by 11:00 CST followed by a gradual decline to ~6.5 ppb h^{-1} by 15:00 CST. On the other hand, the dry deposition rate of O_3 monotonically increased from ~2 ppb h^{-1} at the beginning of the simulation to ~3 ppb h^{-1} at the end while that of NO_x monotonically decreased from ~0.09 to 0.03 ppb h^{-1} during the same period. This clearly shows that these quantities are highly dependent on the time of the day as well as the photochemical age of the air parcel.

[36] The associated Lagrangian and chemical OPEs calculated using equations (6)–(9) are plotted in Figure 11b. The Lagrangian OPEs include effects of both chemistry and dry deposition while the chemical OPEs are functions of chem-

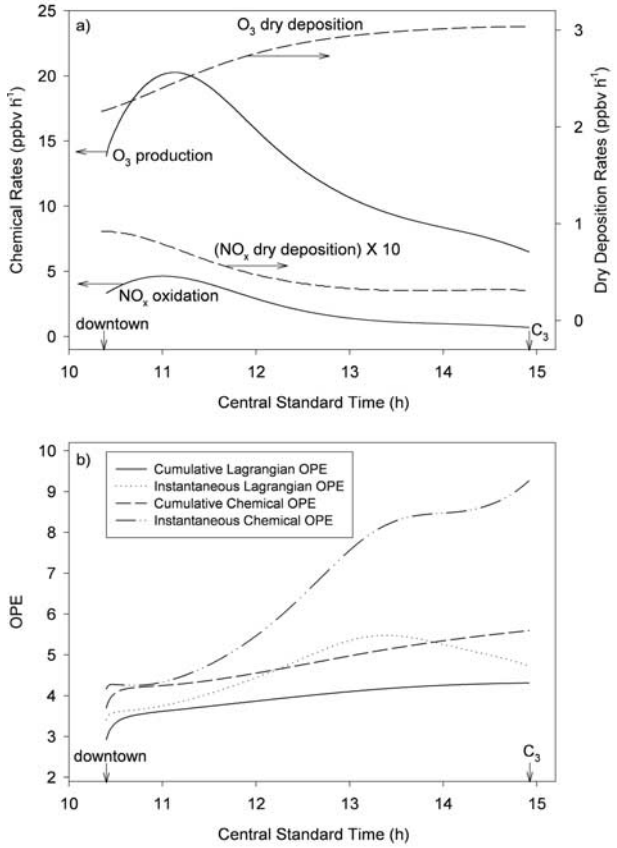

Figure 11. (a) Simulated net chemical and dry deposition rates of O_3 and NO_x along T_3 as a function of time; (b) simulated OPEs along T_3 as a function of time.

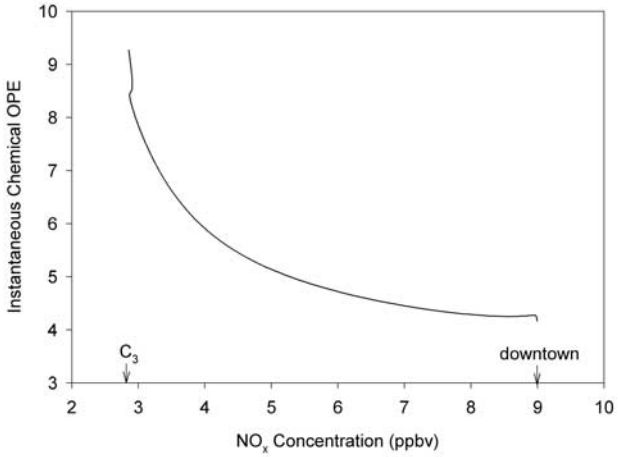

Figure 12. Evolution of the simulated instantaneous chemical OPE in a parcel of air as a function of the simulated NO_x concentration along T_3.

istry only. Because the chemical OPEs do not include dry deposition, they are greater than the corresponding Lagrangian OPEs, and provide upper limits to the efficiency with which O_3 could be produced in the air parcel. Also, note in the plot that both the instantaneous Lagrangian and chemical OPEs increased gradually and were close to their cumulative counterparts until about 11:00 CST when the O_3 production rate reached its maximum, but increased more rapidly than the cumulative OPEs thereafter until ~13:00 CST. This indicates that although the system became "locally" more efficient in producing O_3 as the NO_x concentrations continued to drop, the cumulative OPEs did not increase as rapidly as the instantaneous OPEs because both the O_3 production and NO_x destruction rates monotonically decreased after ~11:00 CST.

[37] While the instantaneous chemical OPE continued to increase, although very slowly, after 13:00 CST, the instantaneous Lagrangian OPE actually decreased during the same period. This is because the dry deposition rate of O_3, which is directly proportional to its concentration, became increasingly important in the "aged" air parcel with high O_3 in which O_3 was being produced at a much lower rate than at noon. It is also worth noting here that the modeled net rate of PAN formation remained positive until the end of the simulation, and therefore the increase in the instantaneous chemical OPE was not due to decomposition of PAN to give back NO_2, but rather due to more efficient production of O_3 at lower NO_x levels as shown in Figure 12. This is consistent with the results of *Daum et al.* [2000] who estimated observation-based instantaneous chemical OPEs in air parcels of different photochemical ages in the Nashville urban plume during the 1995 SOS campaign.

[38] Both cumulative Lagrangian and chemical OPEs increased almost linearly from their initial values of ~3.2 and ~4.0, respectively, and reached ~4.3 and ~5.6, respectively, at C_3. The Lagrangian values are in excellent agreement with the previous estimates by *Sillman et al.* [1998] and *Nunnermacker et al.* [1998] who report values between 3 and 4 for the Nashville urban area. The observed cumulative Lagrangian OPE calculated using equation (2) is ~5.0, and is greater than its modeled counterpart as expected, since the observed value is based on NO_z species, which undergo rapid dry deposition. Although the observed Lagrangian OPE is slightly smaller than the modeled cumulative chemical OPE in the present case, no particular trend may be expected between them. This is because the observed value can exceed the "true" upper limit value represented by cumulative chemical OPE as the NO_z species in the air parcel continue to deplete due to dry deposition while the photochemical production of O_3 slows down as the afternoon progresses. The various observation-based and modeled OPEs are summarized in Table 3.

5. Sensitivity Analysis

[39] The Lagrangian box model used in this study has been carefully constrained and evaluated using a variety of observations, and appears to characterize the T_3 trajectory scenario reasonably well. From the above analysis, it is evident that downwind O_3 concentrations in an urban plume depends not only on the emissions of NO_x and VOCs, but on a number of other factors such as dilution, dry deposition, initial and background concentrations, solar radiation, temperature, and possibly other meteorological controls. It is also evident that the cumulative OPE in an air parcel is complex outcome of these factors and displays a nonlinear dependence on NO_x emissions as well as NO_x/VOC emissions ratio. A comprehensive analysis of how changes in each and every one of these factors and their combinations affect the downwind O_3 concentrations is beyond the scope of this report. We focus here on the sensitivity of O_3 production and the associated net cumulative chemical OPE to the plume dilution rate and the emissions of anthropogenic NO_x and VOCs with respect to the T_3 trajectory scenario as the base case.

5.1. Sensitivity to the Dilution Rate

[40] In addition to the no-dilution ($\lambda = 0.0\ s^{-1}$) and base case ($\lambda = 3.1 \times 10^{-5}\ s^{-1}$) simulations discussed above, we performed a high-dilution run with $\lambda = 6.0 \times 10^{-5}\ s^{-1}$. In all three simulations, the initial and background concentrations of all the species and the emissions of primary species were same as the base case levels. A plot of O_3 and NO_x concentrations as a function of downwind processing time (along T_3) for the three scenarios shows that an increase in the dilution rate lowered the NO_x and O_3 concentrations in the urban air parcel. This also lowered the net photochemical O_3 production and NO_x oxidation rates (Figure 13b), implying that dilution not only reduced

Table 3. Comparison of the Different Measures of OPE

OPE	Value	Method
Regression OPE for the entire plume	4.7 ± 1.2	Figure 5a
Cross-plume OPE at C_3	5.5	equation (1)
Observed cumulative Lagrangian OPE at C_3	5.0	equation (2)
Instantaneous Lagrangian[a] OPE at C_3	4.7[c]	equation (6)
Cumulative Lagrangian[a] OPE at C_3	4.3[c]	equation (7)
Instantaneous chemical[b] OPE at C_3	9.3[c]	equation (8)
Cumulative chemical[b] OPE at C_3	5.6[c]	equation (9)

[a]Calculation of Lagrangian OPEs include chemical and dry deposition rates.
[b]Calculation of chemical OPEs include chemical rates only.
[c]The values at C_3 refer to the end-points of the OPE plots in Figure 11b.

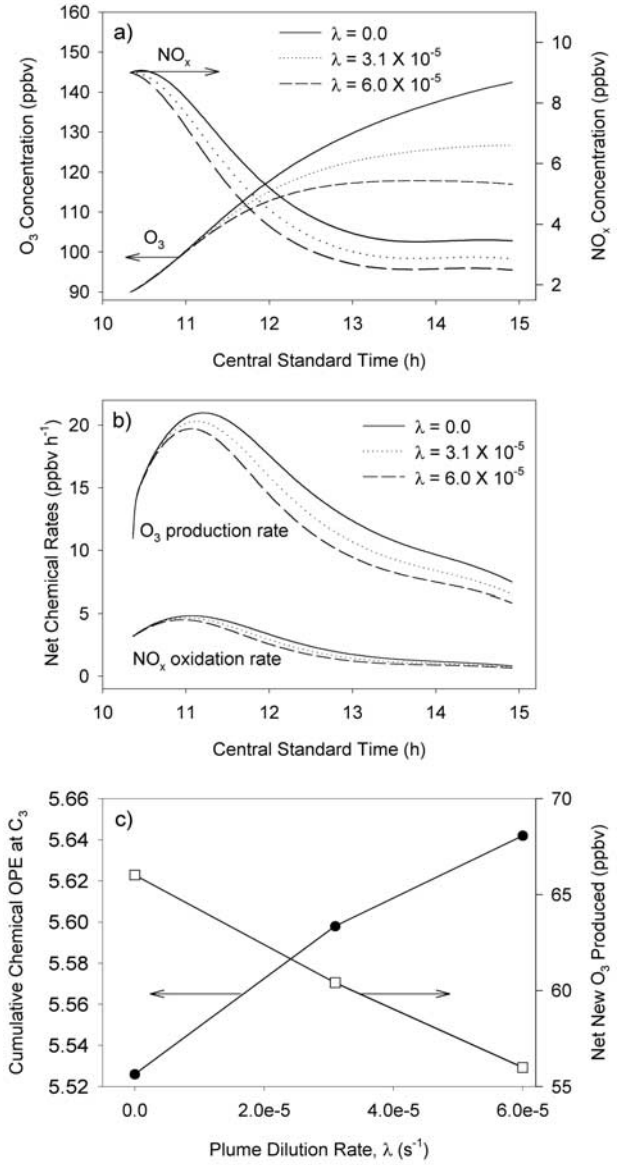

Figure 13. Sensitivity to the plume dilution rate: (a) O_3 and NO_x concentrations along T_3 as a function of time; (b) net chemical production and oxidation rates of O_3 and NO_x, respectively, along T_3 as a function of time; (c) cumulative chemical OPE at C_3 and net new O_3 produced due to photochemistry along T_3 plotted as a function of the plume dilution rate.

the peak O_3 concentrations due to mixing with the background air, but also suppressed the photochemical production of new O_3 in the urban air parcel due to reduced NO_x concentrations along T_3.

[41] Dilution in the context of a box model simulation of an urban plume has the consequence of moving pollutants from inside the urban air parcel to the outside "background" air. Although less net new O_3 is produced in the urban air parcel due to dilution (see Figure 13c), additional O_3 is expected to be formed on the outside as NO_x is being transferred from a high-NO_x, low-OPE environment, to a low-NO_x, high-OPE environment. Figure 13c also shows that for the Nashville plume, there is only a small effect on the net cumulative chemical OPE within the urban air parcel, changing from ~5.64 in the no-dilution case to ~5.52 in the high-dilution case; however, the OPE in the background air would be much higher. Thus the qualitative expectation is that the total amount of O_3 formed from the same emissions of NO_x and VOCs will increase with dilution, while the peak O_3 concentrations will decrease. Two- and three-dimensional models that resolve the cross-wind plume are needed to quantify the overall effect that dilution has on the total amount of O_3 produced as well as its peak concentrations.

5.2. Sensitivity to NO_x and VOC Emissions

[42] We examined the sensitivity of O_3 production within the urban air parcel to the emission rates of NO_x and anthropogenic VOCs along the T_3 trajectory for the base case dilution rate of $\lambda = 3.1 \times 10^{-5}\ s^{-1}$. The base case emission rates were varied by multiplying them with a scaling factor, S_j (where j = NO_x, VOC, or both) ranging from 0.5 to 1.5 (i.e., ±50%). The initial concentrations of NO_x and VOCs were also simultaneously scaled by the same factor on the assumption that they are linearly proportional to their emissions in a well-mixed layer near the source region. Since PAN is a secondary species, its initial and background concentrations would not only depend on local formation, but also on regional-scale transport of its precursors. In the first set of sensitivity runs, the initial and background concentrations of PAN were kept constant at the base case level of 2.0 ppb, assuming that changes in Nashville emissions have negligible impact on the background concentrations of PAN. In the second set of runs, we scaled both the initial and background PAN concentrations as $[PAN] = S_{NO_x} \times S_{VOC} \times [PAN]_{base\ case}$, assuming that changes in Nashville emissions and presumably similar changes in the emissions of other urban areas in the region produce a proportionate change in the background concentrations of PAN. Emissions of isoprene and all other initial and background concentrations remained at the base case levels for all simulations. Results from these two sets of sensitivity runs are discussed below.

5.2.1. Fixed Initial and Background PAN Concentrations

[43] Figure 14a shows the dependence of the cumulative chemical OPE, as defined by equation (9), to the scaling of NO_x emissions only, VOC emissions only, and both NO_x and VOC emissions simultaneously with respect to the base case scenario. Thus each point on the lines in this figure represents the chemical OPE predicted at the end point C_3 (indicated in Figure 4) for the corresponding scaling factor value applied to the base case emissions and initial concentrations as mentioned earlier. The figure shows that OPE decreases at high NO_x concentrations as was predicted by *Liu et al.* [1987] and observed by *Ryerson et al.* [1998, 2001], and increases at high VOC concentrations as observed by *Luria et al.* [2000] and *Ryerson et al.* [2001]. However, it should be also noted that part of the increase of OPE at low S_{NO_x} is due to PAN decomposition to give back NO_2.

[44] Figure 14b shows the corresponding net amount of O_3 photochemically produced in the urban air parcel at C_3 since leaving the downtown area. These curves indicate that the base case scenario is slightly more sensitive to NO_x than

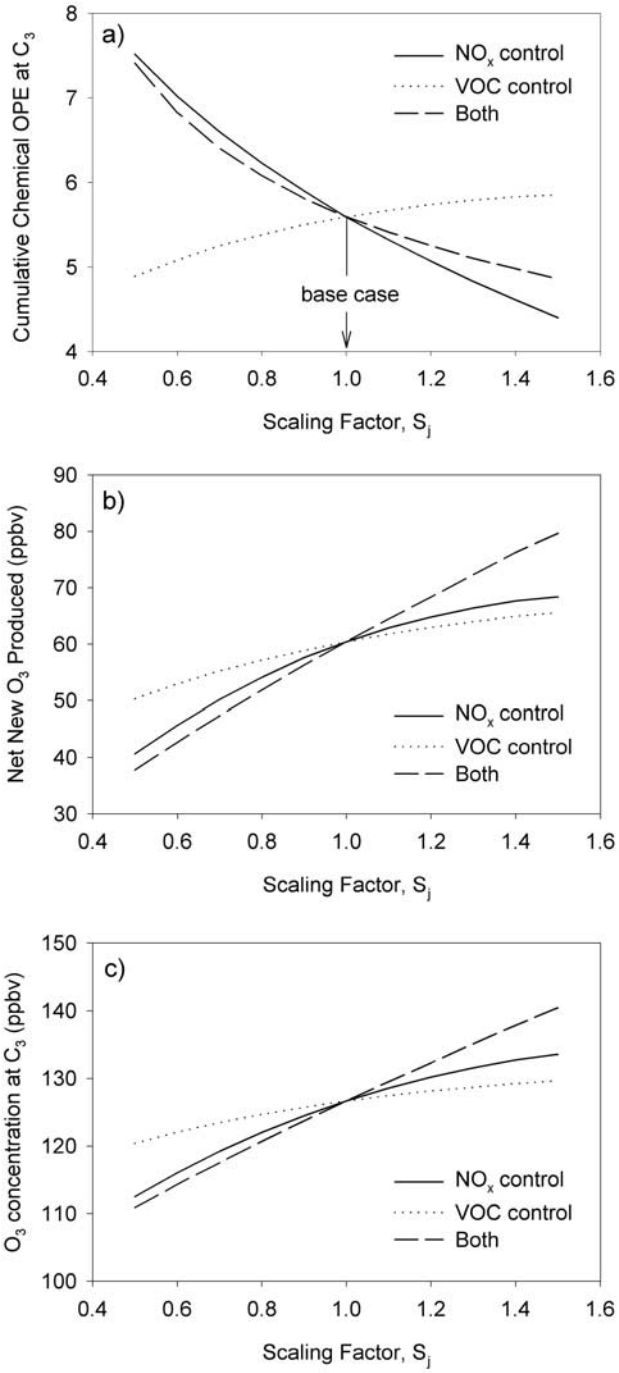

Figure 14. Sensitivity plots for fixed initial and background concentrations of PAN at the base case value of 2.0 ppbv: (a) sensitivity of the cumulative chemical OPE at C_3 to variations in NO_x and VOC emissions and initial concentrations as determined by the appropriate scaling factors; (b) net new O_3 produced due to photochemistry only along T_3 as a function of the scaling factors; (c) O_3 concentrations at C_3 as a function of the scaling factors.

VOC emissions and initial concentrations. The system becomes even more sensitive to NO_x than VOC as the individual scaling factors are reduced with respect to the base case. However, the base case is most sensitive to simultaneous increases or reductions in both NO_x and VOC emissions and initial concentrations. This analysis suggests that a ~10-ppbv reduction in the net photochemical O_3 production from the base case value of ~60 ppbv would require about 20% simultaneous reduction in both NO_x and VOC emissions, or a 30% reduction in NO_x emissions only, or almost 50% reduction in anthropogenic VOC emissions only. This is qualitatively consistent with previous studies which show biogenic VOC as contributing substantially to ozone formation in the Nashville area, with the result that reductions in anthropogenic VOC alone are less effective than they would be in another region with only minimal biogenic input. On the other hand, the net photochemical O_3 production at C_3 would increase by about 5 ppbv if both the NO_x and VOC emissions were to simultaneously increase by just 10%, or by a 20% increase in NO_x emissions only, while nearly 45% increase in the anthropogenic VOC emissions alone is required to produce the same effect. Although increasing NO_x emissions causes a sharp decline in the chemical OPE, such a NO_x-rich plume would become more efficient and produce even more O_3 further downwind as the plume undergoes more dilution with the background air [*Sillman*, 1999]. Also, the chemical OPE and O_3 concentrations in such an urban plume traveling to rural areas would become even less sensitive to anthropogenic VOC control because of the dominating effect of biogenic VOCs. The corresponding downwind O_3 concentrations displayed in Figure 14c show similar sensitivities to the scaling factors as the net O_3 production, although the magnitudes of changes in the concentrations are diminished due to dry deposition at the surface and dilution with the background. Furthermore, the percentage changes in downwind O_3 concentration is also smaller compared to the percentage change in net new O_3 produced for any given value of the scaling factor, because the initial O_3 concentration is rather high (~90 ppbv).

5.2.2. Scaled Initial and Background PAN Concentrations

[45] By scaling the initial and background PAN concentrations as a function of S_{NO_x} and S_{VOC}, the net PAN formation rate remained positive until the end of all the simulations. Figure 15a shows the plot of cumulative net chemical OPE as a function of the scaling factors. As in the fixed PAN runs, the net OPE increased with decrease in NO_x emissions, although not as rapidly. The net OPE for the fixed PAN scenario reached ~7.5 for a 50% reduction in NO_x emissions only while it was ~6.5 for the scaled PAN scenario for the same reduction in NO_x emissions. This is because the increase in the cumulative chemical OPE for the scaled PAN runs is not partially due to the thermal decomposition of PAN to give back NO_2, but entirely due to an increase in the instantaneous chemical OPE as NO_x concentrations decreased. The cumulative net chemical OPE increases more rapidly in the scaled PAN runs than in the fixed PAN runs for the VOC-only control as S_{VOC} increases from 0.5 to 1.5. Again, this is attributed to the lack of net thermal decomposition of PAN to give back NO_2 at low-VOC concentrations while slowing down PAN formation at high VOC concentrations. Interestingly, the cumulative net chemical OPEs for the simultaneous control of both NO_x and VOCs runs showed little sensitivity to the emissions scaling factor. That is behavior can be attributed to the opposing

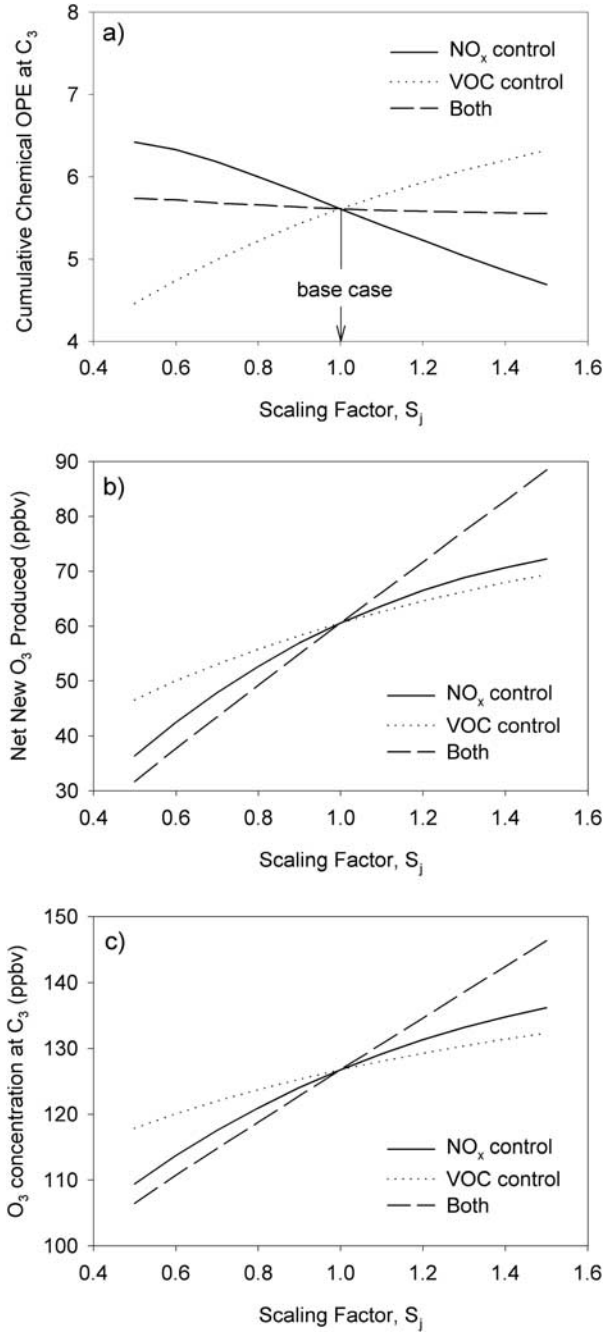

Figure 15. Sensitivity plots for varying initial and background concentrations of PAN as $[PAN] = S_{NO_x} \times S_{VOC} \times [PAN]_{base\ case}$: (a) sensitivity of the cumulative chemical OPE at C_3 to variations in NO_x and VOC emissions and initial concentrations as determined by the appropriate scaling factors; (b) net new O_3 produced due to photochemistry only along T_3 as a function of the scaling factors; (c) O_3 concentrations at C_3 as a function of the scaling factors.

effects of NO_x and VOC emissions on the chemical OPE. In the case of scaled PAN concentrations, these opposing effects are nearly equal in magnitude and tend to cancel each other, thus making the net OPE relatively insensitive to simultaneous reductions or increases in NO_x and VOC emissions.

[46] The net new photochemically produced O_3 for the scaled PAN runs is shown in Figure 15b. In accordance with the OPE sensitivities described above, the net new O_3 production is most sensitive to simultaneous reductions in the NO_x and VOC emissions. Furthermore, the plots show that reductions in the background and initial PAN concentrations result in lower net new O_3 production for the same amount of NO_x and/or VOC reductions than for the fixed PAN concentration runs. On the other hand, increases in PAN concentrations with increase in NO_x and/or VOC emissions produce even higher amounts of new O_3 with increases than for the fixed PAN concentration runs. Corresponding trends are also seen in the downwind concentrations of O_3, although the effects are diminished as before due to dilution and dry deposition (Figure 15c).

5.3. Implications for Evaluating O_3-NO_x-VOC Sensitivity in Urban Plumes

[47] From a regulatory perspective, the central issue of O_3 formation and transport is the extent to which changes in urban emissions of NO_x and VOCs may affect the peak hourly and 8-hourly averaged O_3 concentrations. Contribution of O_3 from urban plumes to the background levels is also of concern. The above analysis shows that O_3 production in an urban plume depends not only on the absolute and relative emissions of NO_x and VOCs in the plume, but also on their background concentrations and the dilution rate. Background concentration of species such as PAN, which can thermally decompose to give back NO_2, appears to be important in the effectiveness of emission control strategies; higher background PAN concentrations would make it harder to control net new O_3 production from the emissions of NO_x and VOCs in the urban area. Since O_3 production and NO_x oxidation rates depend strongly on the time of the day, the net amount of O_3 produced in an urban plume would also depend on the timing of the emissions. The net cumulative chemical OPE associated with O_3 production in the urban plume also appears to be a complex, nonlinear function of these factors.

[48] Observations of OPE such as described by *Ryerson et al.* [2001] suggest a general strategy for reducing O_3 by shifting NO_x emissions from power plant point sources with high OPE to ones with low OPE: based on the surrounding biogenic emissions and the size of the NO_x emitting point source. Observation-based OPEs, however, can only provide a partial answer to the problems of designing an O_3 control strategy. One needs to know the nonlinear response in O_3 to a wide range of changes in NO_x and VOC emission rates, such as might be envisioned in O_3 control strategies for urban areas. Urban plumes are significantly more complex than power plant plumes in terms of (1) chemical composition of the anthropogenic VOC emissions; (2) NO_x/VOC emissions ratios; (3) influence of biogenic VOC emissions; and (4) spatial and temporal variability in all these emissions. Because the OPE exhibits a nonlinear dependence on emissions, background concentrations, and meteorological effects, it would be difficult to rely on observations alone to map out the nonlinear response of O_3 to a wide span of NO_x and VOC emission changes. It is also difficult to fully characterize the effects of regional-scale transport of O_3

and its precursors on local O_3 production in an urban area from observations alone [*Fast et al.*, 2002]. A combination of observation-based analyses and modeling techniques is therefore needed.

[49] However, if the models are to be believed, they must not only reproduce the observed concentrations of O_3, NO_x, NO_y, and the key VOCs, but also agree with the observations of the OPE. The overall model reliability depends on a number of factors including: (1) the accuracy of the available emission inventories; (2) the fidelity of the photochemical mechanisms; and (3) the accuracy of the important meteorological effects (solar radiation, transport, and mixing) in the model. Thus the model evaluation and validation process should include comparisons of as many key variables (chemical and meteorological) as possible as well as evaluation of sensitivity indicators such as the OPE and H_2O_2/NO_z ratio against observed values [*Sillman*, 1999]. Although a number of species were used to evaluate the performance of the Lagrangian box model used in this study, comparisons between the predicted concentrations and observations were possible only at the end of the air parcel trajectory simulation (at C_3), where aircraft observations were made. Unfortunately, it was not possible to corroborate the modeled rates of O_3 production and NO_x depletion in the Lagrangian urban air parcel due a lack of time-resolved observations in the urban plume. For this reason, the accuracy of the approximations and assumptions associated with transport, dilution, and other dynamic processes in the model could not be independently confirmed. It is therefore necessary to obtain Lagrangian measurements in the urban plume for evaluating and validating the fidelity of the chemical kinetic and dynamic processes in the models. Only such a model that is properly constrained and well evaluated using different types of observations as described above may be reliably used to predict O_3-NO_x-VOC sensitivity for designing effective regulatory strategies. Conversely, a model that is improperly constrained and inadequately evaluated may reproduce certain observations for erroneous reasons, and is therefore not only ineffective, but also risky if used for policy purposes.

6. Summary and Conclusions

[50] Aircraft and surface measurements taken in the Nashville area as part of the 1999 Southern Oxidant Study field campaign were analyzed to understand the behavior of ozone production efficiency and NO_x depletion in an urban plume. The plume centerline was estimated based on the peak NO_y concentrations, and the air parcel ages as a function of downwind distance from the source area was derived from back-trajectories calculated using nearby wind profiler measurements. This information was used to calculate different types of observation-based OPEs as well as drive a Lagrangian box model, which served as a key tool in our analysis. Particular care was taken in selecting or estimating the various model inputs including the initial and background concentrations, emissions, photolysis rates, and dilution rate as well as the data to evaluate the model. Although many assumptions and uncertainties exist in initializing and constraining the model, it does quite well in simulating the concentrations of O_3, NO_x, NO_z, and key VOCs in a chosen air parcel in the plume as it advected downwind along its calculated trajectory. The model was then used to calculate the O_3 production and NO_x depletion rates in the air parcel along with the associated instantaneous and cumulative ozone production efficiencies (Lagrangian and chemical). A sensitivity study was also performed to investigate the effects of dilution rate and emissions of NO_x and VOCs on downwind O_3 concentration and cumulative chemical OPE. Our conclusions, based on these analyses, are as follows:

[51] (1) The observation-based regression OPE for the 22 June 1999, Nashville urban plume was found to be 4.7 ± 1.2, and is consistent with previous estimates [*St. John et al.*, 1998; *Nunnermacker et al.*, 1998]. The cross-plume OPEs calculated along the plume centerline with respect to plume edge conditions were found to increase with the air parcel age, which was estimated as the time the air parcel took to travel from the downtown area.

[52] (2) The model-based instantaneous O_3 production and NO_x oxidation rates along a selected air parcel trajectory were dependent on the time of day (photolysis rates) as well as the photochemical age of the air parcel. The rapid increase in the associated model-based instantaneous chemical OPE revealed that the air parcel became more efficient in O_3 production as NO_x concentrations decreased due to oxidation. However, the cumulative Lagrangian and chemical OPEs increased relatively slower due to decrease in both the O_3 production and NO_x oxidation rates as the air parcel aged. The modeled cumulative OPEs were consistent with the observation-based values with the expected biases.

[53] (3) The sensitivity analyses show that while the modeled chemical OPE appears to be relatively insensitive to the dilution rate for the present episode, it responds nonlinearly to changes in NO_x and anthropogenic VOC emissions. It decreases at high NO_x, increases at high VOC and vice versa, which are consistent with previous studies [*Liu et al.*, 1987; *Lin et al.*, 1988; *Luria et al.*, 2000; *Daum et al.*, 2000; *Ryerson et al.*, 1998, 2001]. The corresponding downwind O_3 concentrations responded in a nonlinear fashion as well. Moreover, because of high biogenic emissions in the Nashville area, reductions in anthropogenic VOCs alone appeared to be less effective in reducing the net O_3 formation than they would be in another region with only minimal biogenic input, indicating that effective control strategies must be tailored by region. These results are also found to be sensitive to the initial and background PAN concentrations, and their effects must be taken into account in formulating O_3 control strategies for urban plumes.

[54] (4) It is evident that observations can only provide a partial answer to the problems of designing O_3 control strategies for urban areas. Because of the spatial and temporal variability and complexity in the composition of the anthropogenic VOC and NO_x emissions in urban plumes, it would be difficult to rely only on observations to map out the nonlinear response of O_3 to a wide span of NO_x and VOC emission changes, such as might be envisioned for O_3 control strategies. A combination of observation-based analyses and modeling techniques is therefore needed for evaluating O_3-NO_x-VOC sensitivity.

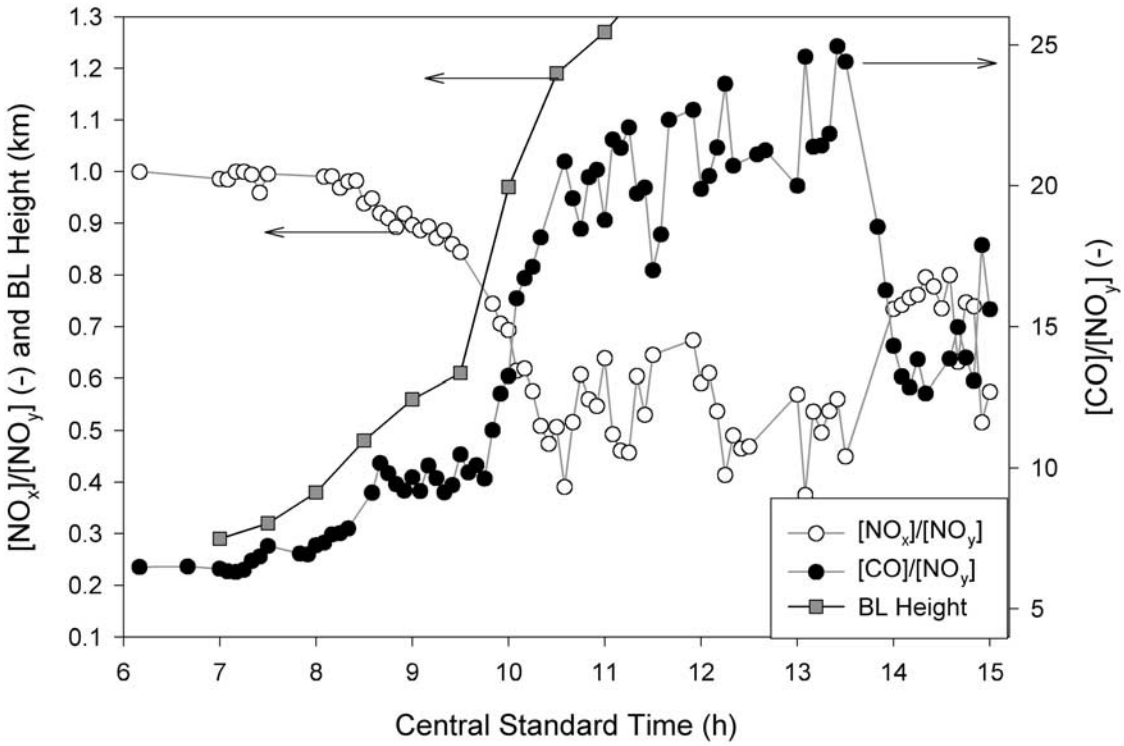

Figure A1. Time series of NO_x/NO_y and CO/NO_y concentration ratios measured at the Polk Building site, and the boundary layer height observed at CFA.

[55] (5) We agree with *Sillman* [1999] that models must be properly constrained and rigorously evaluated using observations before they reliably predict the O_3-NO_x-VOC sensitivity. The model evaluation and validation process should include comparisons of O_3, NO_x, NO_z, VOCs, and sensitivity indicators such as OPE and H_2O_2/NO_z ratio with observed values. It is also necessary to evaluate the modeled rates at which these key chemical species accumulate, react, and disperse in different air parcels against Lagrangian measurements in an urban plume to substantiate the fidelity of the various chemical and dynamic processes represented in models.

[56] (6) Last, due to its simplicity and computational efficiency, Lagrangian models could serve as a useful intermediate step for interpreting aircraft observations and extracting valuable information on photochemical aging, lifetimes of important species, and O_3-NO_x-VOC sensitivity in an urban plume. Insights gained from this exercise should prove useful in carrying out more comprehensive analyses with 3-D Eulerian models.

Appendix A: Estimation of the CO/NO_x Emissions Ratio

[57] Figure A1 shows NO_x/NO_y and CO/NO_y concentration ratios observed atop the Polk Building as a function of local time. The NO_x/NO_y concentration ratio was ~1 during the early morning hours, slowly decreased to about 0.85 by 9:30 CST, and rapidly decreased to less than 0.5 in the next hour. At the same time, the CO/NO_y concentration ratio increased gradually from ~6.5 to ~10.5, and was greater than 20 by 10:30 CST. The trends in these ratios are highly correlated with the evolution of the boundary layer height, also shown in Figure A1, suggesting that the change in these ratios can be explained on the basis of mixing of the freshly polluted boundary layer air with the aged background air aloft. The CO/NO_y concentration ratio in aged air aloft is much larger than in a freshly polluted air parcel because of continued depletion of NO_y in aged air due to dry deposition prior to being decoupled from the surface. In contrast, the conversion of NO_x to NO_z would result in a smaller NO_x/NO_y concentration ratio in photochemically aged air than in freshly polluted air. These qualitative arguments support the hypothesis that as the freshly polluted boundary layer air mixed with the aged air aloft, the CO/NO_y ratio increased and NO_x/NO_y ratio decreased at a rate governed by the growth of the boundary layer.

[58] The ratio of CO to NO_x emissions can be derived from the Polk Building observations and the governing equation for a simple Eulerian box model with a constant mixed layer height, H [*Seinfeld and Pandis*, 1998].

$$\frac{dC_i}{dt} = \frac{E_i}{H} + R_i - \frac{v_{d,i}}{H} C_i + \frac{(C_{i,b} - C_i)}{\tau_r} \quad \text{for constant } H, \qquad \text{(A1)}$$

where τ_r is the residence time of air in a box of height H (boundary layer height) and arbitrary surface area; other symbols have the same meaning as defined earlier. One can apply this model to the downtown area for the early morning period between 6:00 and 7:30 CST when the boundary layer height was relatively constant. During this period, the NO_x/NO_y concentration ratio was greater than

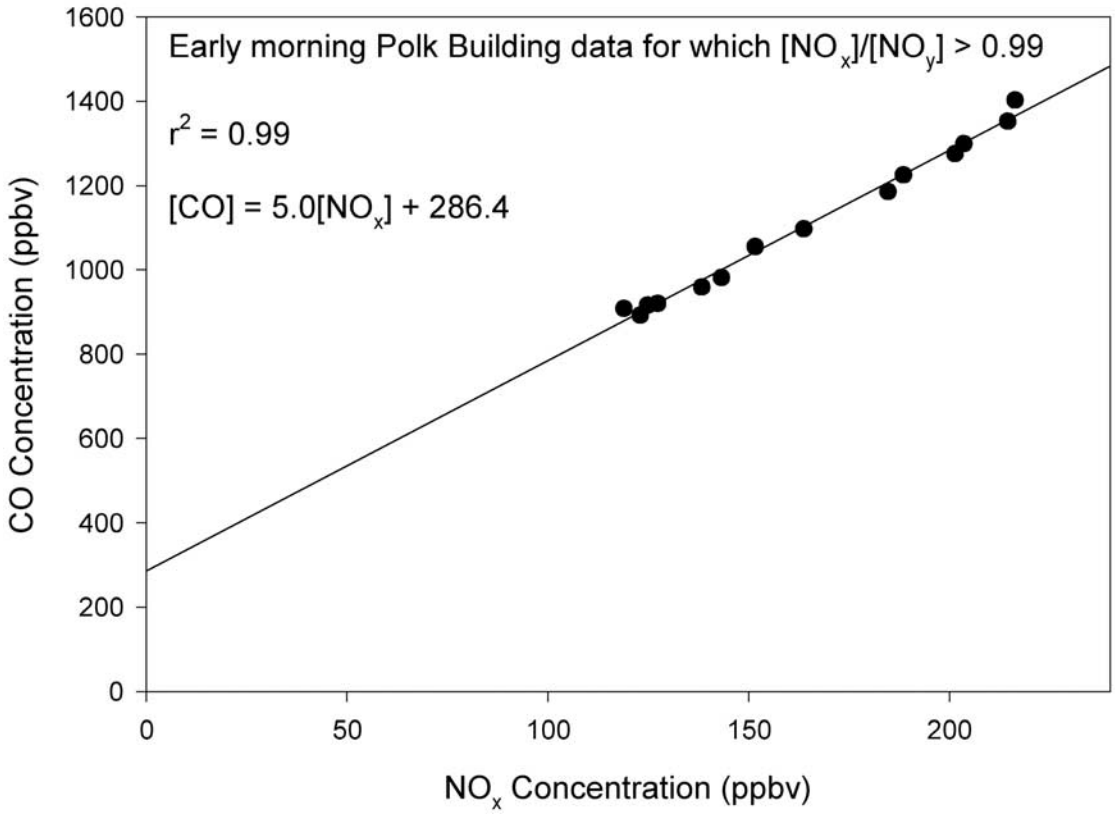

Figure A2. Correlation plot of CO and NO_x concentrations observed early morning at Polk Building. The data are restricted to the condition $[NO_x]/[NO_y] > 0.99$.

0.99 (i.e., $NO_x \approx NO_y$), indicating negligible loss of NO_x due to chemical reaction or dilution due to mixing with the aged background air. It is also reasonable to assume that dry deposition loss of NO_x is negligible compared to the large-NO_x emission rate in the downtown area. We extend these assumptions to CO, which is much less reactive than NO_x. Under these conditions, the right-hand side of equation (A1) reduces to just the emissions term, which can be easily integrated with initial conditions $C_i(0) = C_i^0$, resulting in:

$$C_i = C_i^0 + \frac{E_i}{H}\Delta t. \tag{A2}$$

One can then derive the relationship between the CO and NO_x concentrations through the emissions ratio (E_{CO}/E_{NO_x}) as shown below.

$$C_{CO} = \frac{E_{CO}}{E_{NO_x}} C_{NO_x} + \left(C_{CO}^0 - \frac{E_{CO}}{E_{NO_x}} C_{NO_x}^0 \right). \tag{A3}$$

This relationship is independent of the integration time (Δt) and H, and a plot of C_{CO} versus C_{NO_x} will yield a straight line with a slope equal to the emissions ratio. The resulting plot is shown in Figure A2, yielding a value of $E_{CO}/E_{NO_x} = 5.0 \pm 0.3$ which we have used to calculate the CO emissions from the available NO_x emissions. This result is also consistent with the recent findings of *Parrish et al.* [2002].

[59] **Acknowledgments.** We thank the G-1 pilots (Bob Hannigan, Dick Hone, and Mike Warren) and the flight support crew (John Hubbe, Vic Morris, and John Schmelzer) from PNNL for once again translating our scientific needs into safe flight plans with the G-1. We thank Daniella Zedda and Bob Plastridge of BMI for assistance with airborne PAN observations. In addition to the aircraft measurements, this work involved measurements by many other investigators at the Polk Building (PB) and Cornelia Fort Air Park (CFA) surface sites. We are particularly grateful to Ken Olszyna, Air, Land & Water Sciences, Tennessee Valley Authority, for the chemistry and water vapor data at PB; Wayne Angevine of NOAA for the wind profiler data at CFA; R.E. Shetter of NCAR for the photolysis frequencies data at CFA; and A. Fried of NCAR for HCHO data at CFA. We thank Richard Easter of PNNL for helpful discussions on plume dilution rate calculations; Jerome Fast of PNNL for assistance in using the SMOKE emission inventory; Jim Barnard of PNNL for performing the Fast-*J* calculations; Yulong Xie of PNNL for assistance with statistical analysis; and the two anonymous reviewers for their careful review of the manuscript and many helpful suggestions. Finally, we thank the Tennessee Department of Public Health for use of their facilities. The Atmospheric Chemistry Program within the Office of Biological and Environmental Research of DOE provided much of the support for our participation in the Nashville field and analysis activities and for the G-1 aircraft. Work by Brookhaven National Laboratory was performed under contracts DE-AC02-98CH10886 and DE-AC06-76RLO 1830. The U.S. Environmental Protection Agency through its Office of Research and Development partially funded and collaborated in the research described here under contract CQ829757 to the National Caucus and Center on Black Aged. It has been subjected for Agency review and approved for publication. Pacific Northwest National Laboratory is operated for the U.S. Department of Energy by Battelle Memorial Institute under contract DE-AC06-76RLO 1830.

References

Ackman, R. J., The flame ionization detector: Further comments on molecular breakdown and fundamental group response, *J. Gas Chromatogr.*, *6*, 497–501, 1968.

Altshuller, A. P., The role of nitrogen oxides in nonurban ozone formation in the planetary boundary layer over N America, W Europe and adjacent areas of ocean, *Atmos. Environ.*, *20*, 245–268, 1986.

Angevine, W. M., A. B. White, C. J. Senff, M. Trainer, and R.M. Banta, Urban-rural contrasts in mixing height and cloudiness over Nashville in

1999, *J. Geophys. Res.*, *108*(D3), 4092, doi:10.1029/2001JD001061, 2003.

Apel, E. C., J. G. Calvert, and F. C. Fehsenfeld, The non-methane hydrocarbon intercomparison experiment (NOMHICE): Tasks 1 and 2, *J. Geophys. Res.*, *99*, 16,651–16,664, 1994.

Berkowitz, C. M., and W. J. Shaw, Airborne measurements of boundary layer chemistry during the Southern Oxidant Study: A case study, *J. Geophys. Res.*, *102*, 12,795–12,804, 1997.

Berkowitz, C. M., J. D. Fast, S. Springston, J. M. Hubbe, R. A. Plastridge, R. Larson, C. W. Spicer, and P. Doskey, Formation mechanisms and chemical characteristics of elevated photochemical layers over the Northeast United States, *J. Geophys. Res.*, *103*, 10,631–10,647, 1998.

Blades, A. T., Ion formation in hydrogen flames, *Can. J. Chem.*, *54*, 2919–2924, 1976.

Carter, W. P. L., Condensed atmospheric photooxidation mechanisms for isoprene, *Atmos. Environ.*, *30*, 4275–4290, 1996.

Cowling, E. B., W. L. Chameides, C. S. Kiang, F. C. Fehsenfeld, and J. F. Meagher, Introduction to special section: Southern Oxidants Study Nashville/Middle Tennessee Ozone Study, *J. Geophys. Res.*, *103*, 22,209–22,212, 1998.

Daum, P. H., L. I. Kleinman, L. Newman, W. T. Luke, J. Weinstein-Lloyd, C. M. Berkowitz, and K. M. Busness, Chemical and physical properties of anthropogenic pollutants transported over the North Atlantic during NARE, *J. Geophys. Res.*, *101*, 29,029–29,042, 1996.

Daum, P. H., L. Kleinman, D. G. Imre, L. J. Nunnermacker, Y.-N. Lee, S. R. Springston, and L. Newman, Analysis of the processing of Nashville urban emissions on July 3 and July 18, 1995, *J. Geophys. Res.*, *105*, 9155–9164, 2000.

Doskey, P. V., and H. M. Bialk, Automated sampler for the measurement of non-methane organic compounds, *Environ. Sci. Technol.*, *35*, 591–594, 2001.

Duncan, B. N., and W. L. Chameides, Effects of urban emission control strategies on the export of ozone and ozone precursors from the urban atmosphere to the troposphere, *J. Geophys. Res.*, *103*, 28,159–28,179, 1998.

Fast, J. D., R. A. Zaveri, X. Bian, E. G. Chapman, and R. C. Easter, Effect of regional-scale transport on oxidants in the vicinity of Philadelphia during the 1999 NE-OPS field campaign, *J. Geophys. Res.*, *107*(D16), 4307, 10.1029/2001JD000980, 2002.

Frost, G. J., et al., Photochemical ozone production in the rural southeastern United States during the 1990 Rural Oxidants in the Southern Environment (ROSE) program, *J. Geophys. Res.*, *103*, 22,491–22,508, 1998.

Gery, M. W., G. Z. Whitten, J. P. Killus, and M. C. Dodge, A photochemical kinetics mechanism for urban and regional scale computer modeling, *J. Geophys. Res.*, *94*, 12,925–12,956, 1989.

Gillani, N. V., J. F. Meagher, R. J. Valente, R. E. Imhoff, R. L. Tanner, and M. Luria, Relative production of ozone and nitrates in urban and rural power plant plumes, 1, Composite results based on data from 10 field measurement days, *J. Geophys. Res.*, *103*, 22,593–22,615, 1998a.

Gillani, N. V., M. Luria, R. J. Valente, R. L. Tanner, R. E. Imhoff, and J. F. Meagher, Loss rate of NO_y from a power plant plume based on aircraft measurements, *J. Geophys. Res.*, *103*, 22,585–22,592, 1998b.

Hindmarsh, A. C., ODEPACK: A systematized collection of ode solvers, in *Scientific Computing*, edited by R. S. Stepleman, pp. 55–64, North-Holland, New York, 1983.

Houyoux, M. R., J. M. Vukovich, C. J. Coats Jr., N. W. Wheeler, and P. S. Kasibhatla, Emission inventory development and processing for the Seasonal Model for Regional Air Quality (SMRAQ) project, *J. Geophys. Res.*, *105*, 9079–9090, 2000.

Imhoff, R. E., R. Valente, J. F. Meagher, and M. Luria, The production of O_3 in an urban plume: Airborne sampling of the Atlanta urban plume, *Atmos. Environ.*, *29*, 2349–2358, 1995.

Jobson, B. T., G. J. Frost, S. A. McKeen, T. B. Ryerson, M. P. Buhr, D. D. Parrish, M. Trainer, and F. C. Fehsenfeld, Hydrogen peroxide dry deposition lifetime determined from observed loss rates in a power plant plume, *J. Geophys. Res.*, *103*, 22,617–22,628, 1998.

Kleinman, L. I., et al., Ozone formation at a rural site in the southeastern United States, *J. Geophys. Res.*, *99*, 3469–3482, 1994.

Kleinman, L. I., P. H. Daum, Y.-N. Lee, L. J. Nunnermacker, S. R. Springston, J. Weinstein-Lloyd, and J. Rudolph, Ozone production efficiency in an urban area, *J. Geophys. Res.*, *107*(D23), 4733, doi:10.1029/2002JD002529, 2002.

Leveque, R. E., Determination of C_3–C_8 hydrocarbons in naphtha and reformates utilizing capillary column gas chromatography, *Anal. Chem.*, *39*, 1811–1818, 1967.

Lin, X., M. Trainer, and S. C. Liu, On the nonlinearity of tropospheric ozone, *J. Geophys. Res.*, *93*, 15,879–15,888, 1988.

Liu, S. C., M. Trainer, F. C. Fehsenfeld, D. D. Parrish, E. J. Williams, D. W. Fahley, G. Hubler, and P. C. Murphy, Ozone production in the rural troposphere and the implications for regional and global ozone distributions, *J. Geophys. Res.*, *92*, 4191–4207, 1987.

Lonneman, W. A., Comparison of hydrocarbon composition in Los Angeles for the years 1968 and 1997, Measurement of toxic and related air pollutants, Proceedings of a Specialty Conference, Cary, N. C., Sept. 1 –3 , pp. 356–365, 1998.

Luke, W. T., T. B. Watson, K. J. Olszynna, R. L. Gunter, R. T. McMillen, D. L. Wellman, and S. W. Wilkison, A comparison of airborne and surface trace gas measurements during the Southern Oxidants Study (SOS), *J. Geophys. Res.*, *103*, 22,317–22,337, 1998.

Luria, M., R. L. Tanner, R. E. Imhoff, R. J. Valente, E. M. Bailey, and S. F. Mueller, Influence of natural hydrocarbons on ozone formation in an isolated power plant plume, *J. Geophys. Res.*, *105*, 9177–9188, 2000.

Nunnermacker, L. J., et al., Characterization of the Nashville urban plume on July 3 and July 18, 1995, *J. Geophys. Res.*, *103*, 28,129–28,148, 1998.

Nunnermacker, L. J., L. I. Kleinman, D. Imre, P. H. Daum, Y.-N. Lee, S. R. Springston, and L. Newman, NO_y lifetimes and O_3 production efficiencies in urban and power plant plumes: Analysis of field data, *J. Geophys. Res.*, *105*, 9165–9176, 2000.

Olszyna, K. J., NARSTO SOS99NASH TVA Surface Meteorology and Chemistry Data, 2002. (Available online at http://eosweb.larc.nasa.gov/project/narsto/table_narsto.html, Langley DAAC, Hampton, Va.).

Olszyna, K. J., E. M. Bailey, R. Simonaitis, and J. F. Meagher, O_3 and NO_y relationships at a rural site, *J. Geophys. Res.*, *99*, 14,557–14,563, 1994.

Parrish, D. D., M. Trainer, D. Hereid, E. J. Williams, K. J. Olszyna, R. A. Harley, J. F. Meagher, and F. C. Fehsenfeld, Decadal change in carbon monoxide to nitrogen oxide ratio in U.S. vehicular emissions, *J. Geophys. Res.*, *107*(D12), 4140, 10.1029/2001JD000720, 2002.

Pielke, R. A., et al., A comprehensive meteorological modeling system-RAMS, *Meteorol. Atmos. Phys.*, *49*, 69–91, 1992.

Rickard, A. R., G. Salisbury, P. S. Monks, A. C. Lewis, S. Baugitte, B. J. Bandy, K. C. Clemitshaw, and S. A. Penkett, Comparison of measured ozone production efficiencies in the marine boundary layer at two European coastal sites under different pollution regimes, *J. Atmos. Chem.*, *43*, 107–134, 2002.

Ryerson, T. B., et al., Emissions lifetimes and ozone formation in power plant plumes, *J. Geophys. Res.*, *103*, 22,569–22,583, 1998.

Ryerson, T. B., et al., Observations of ozone formation in power plant plumes and implications for ozone control strategies, *Science*, *292*, 719–723, 2001.

Seinfeld, J. H., and S. N. Pandis, *Atmospheric Chemistry and Physics: From Air Pollution to Climate Change*, John Wiley, Hoboken, N. J., 1998.

Shetter, R. E., L. Cinquini, B. L. Lefer, S. R. Hall, and S. Madronich, Comparison of airborne measured and calculated spectral actinic flux and derived photolysis frequencies during the PEM Tropics B mission, *J. Geophys. Res.*, *108*(D2), 8234, doi:10.1029/2001JD001320, 2003.

Sillman, S., The relation between ozone, NO_x, and hydrocarbons in urban and polluted rural environments, *Atmos. Environ.*, *33*, 1821–1845, 1999.

Sillman, S., Ozone production efficiency and loss of NO_x in power plant plumes: Photochemical model and interpretation of measurements in Tennessee, *J. Geophys. Res.*, *105*, 9189–9202, 2000.

Sillman, S., D. He, M. R. Pippin, P. H. Daum, D. G. Imre, L. I. Kleinman, J. H. Lee, and J. Weinstein-Lloyd, Model correlations for ozone, reactive nitrogen, and peroxides for Nashville in comparison with measurements: Implications for O_3-NO_x-hydrocarbon chemistry, *J. Geophys. Res.*, *103*, 22,629–22,644, 1998.

Solomon, P., E. Cowling, G. Hidy, and C. Furiness, Comparison of scientific findings from major ozone field studies in North America and Europe, *Atmos. Environ.*, *34*, 1885–1920, 2000.

St. John, J. C., W. L. Chameides, and R. Saylor, Role of anthropogenic NO_x and VOC as ozone precursors: A case study from the SOS Nashville/Middle Tennessee Ozone Study, *J. Geophys. Res.*, *103*, 22,415–22,423, 1998.

Trainer, M., et al., Correlation of ozone with NO_y in photochemically aged air, *J. Geophys. Res.*, *98*, 2917–2925, 1993.

Trainer, M., B. A. Ridley, M. P. Buhr, G. Kok, J. Walega, G. Hübler, D. D. Parrish, and F. C. Fehsenfeld, Regional ozone and urban plumes in the southeastern United States: Birmingham, a case study, *J. Geophys. Res.*, *100*, 18,823–18,834, 1995.

Trainer, M., D. D. Parrish, P. D. Goldan, J. Roberts, and F. C. Fehsenfeld, Review of observation-based analysis of the regional factors influencing ozone concentrations, *Atmos. Environ.*, *34*, 2045–2061, 2000.

Wild, O., X. Zhu, and M. J. Prather, Fast-*J*: Accurate simulation of in- and below-cloud photolysis in tropospheric chemical models, *J. Atmos. Chem.*, *37*, 245–282, 2000.

Zaveri, R. A., and L. K. Peters, A new lumped structure photochemical mechanism for large-scale applications, *J. Geophys. Res.*, *104*, 30,387–30,415, 1999.,

C. M. Berkowitz and R. A. Zaveri, Atmospheric Sciences and Global Change Division, Pacific Northwest National Laboratory, Battelle Boulevard, MSIN K9-30, P.O. Box 999, Richland, WA 99352, USA. (carl.berkowitz@pnl.gov; rahul.zaveri@pnl.gov)

P. V. Doskey, Environmental Research Division, Argonne National Laboratory, Argonne, IL 60439, USA. (pvdoskey@anl.gov)

L. I. Kleinman and S. R. Springston, Environmental Sciences Department, Brookhaven National Laboratory, Upton, NY 11973, USA. (kleinman@bnl.gov; srs@bnl.gov)

W. A. Lonneman, National Exposure Research Laboratory, Senior Environmental Employment Program, U.S. Environmental Protection Agency, Research Triangle Park, NC 27711, USA. (lonneman.bill@epamail.epa.gov)

C. W. Spicer, Atmospheric Science and Applied Technology Department, Battelle Memorial Institute, Columbus, OH 43201, USA. (spicerc@battelle.org)